A Numerical Study of Moisture Forecast in the Planetary Boundary Layer

By

T.S. Chen

Department of Atmospheric Science
Colorado State University
Fort Collins, Colorado

Colorado
State
University

Department of
Atmospheric Science

Paper No. 198

A NUMERICAL STUDY OF MOISTURE FORECAST

IN THE PLANETARY BOUNDARY LAYER

by

T. S. Chen

Department of Atmospheric Science
Colorado State University
Fort Collins, Colorado

March, 1973

Atmospheric Science Paper No. 198

PREFACE

A potential numerical approach to the problems of automotive lead transport through the atmosphere in the planetary boundary layer has motivated the author's strong interest in completing this manuscript although the main part of computation was basically performed in 1969 while the author was visiting the National Center for Atmospheric Research, Boulder, Colorado. This paper has not previously been considered for publication nor published in any form.

The need for better prediction of air pollution concentrations within urban areas in general, or the lead transport near highways in particular, has encouraged the development of various transport models capable of describing both temporal and spatial variations of dispersion parameters. Two principal problems must be resolved during the development of such models: (1) a computational procedure must be formulated which yields stable solutions and which incorporates adequate detail of the phenomena of interest over appropriate time and spatial scales, and (2) appropriate and consistent profiles of meteorological parameters must be chosen for use as model input data.

This paper touches upon subjects quite closely related to these two problems (see abstract). In the problems of lead transport, the emissions generally occur near ground level (excluding the natural occurrence of Pb^{210}). Variations in mixing rate and horizontal velocity with height are of primary importance. These factors suit this transport problem well to a description derived from the tracer equation which is identical to our moisture transport equation dealing with specific humidity instead of the lead emitted into the environment through automotive exhaust.

Application of the topographical coordinate in this paper enables one to account for the effects of spatial variations in surface roughness, and consideration of latent heat release allows for the variation of thermal characteristics in the planetary boundary layer. Such a consideration in the model is essential to any diffusion problem in practice.

The application envisioned is a complete system describing the automotive lead transport model which can be fundamentally derived from the present work. For example, a hypothesis concerning the influence of upper level inversion height on the vertical diffusivity profile can be made such that the combined effects of mixing height and atmospheric stability can be simulated.

ABSTRACT

A dynamical forecast model is applied to study the moisture variation in the planetary boundary layer under the chosen synoptic condition. The observed 12-hour moisture patterns are compared with the forecast patterns.

Four numerical experiments, using the same initial data on 0600 CST, March 25, 1967, are made. However, in one case only the effects of evaporation from the Gulf of Mexico, and the latent heat release are considered in the model, whereas in the rest of the cases, the topographical effects are also included.

The results indicate that: (a) The moisture tongue shows a good correspondence in location between the forecast and observed values, at 200 meter-level above the ground. (b) The ridge line of the forecast moisture patterns display a tendency of tilting westward when compared with the initial observed values. The degree of tilting depends, very closely, on the speed of the cold front. (c) The forecast moisture in the central U. S. proves to be acceptable, but in the eastern U. S. along the Appalachian Mountains the error is about 2 gm kg^{-1}. (d) For the 12-hour forecast in the central U. S. region, the latent heat release seems to be more important than the evaporation effect.

TABLE OF CONTENTS

1.0 Introduction

The basis for achieving accurate local area forecasts often rests upon the ability of the forecaster to project rapidly changing fields of meteorological variables forward in time from current mesoscale analysis. This objective is seldom realized in actual practice due to a number of varied and complex requirements. Among the prime requirements is the need for a fine-mesh dynamical model which is capable of generating realistic forecasts, including boundary layer interactions with the large scale environment. In addition to the theoretical problems involved, such a model would also require frequent and detailed observations from a dense network of surface and upper air stations. However, the present network of observations, in particular upper air soundings, is too coarse to obtain reasonably accurate and necessary input data as initial conditions for such purposes.

Nevertheless, the above difficulties were partially resolved when Ooyama (1963) first successfully parameterized cumulus convection into the tropical cyclone model. He assumed that the rate of total heat production by convective clouds in a vertical column is proportional to the supply of water vapor in the column by the large scale horizontal convergence in the surface boundary layer. Thus he related the heating by cumulus convection to the dynamics of the large scale circulation through surface friction. By a perturbation analysis he was able to describe a disturbance similar to a tropical cyclone with respect to the growth rate and the preferred scale. It was then possible, to represent statistically the small scale convective motion in terms of parameters of large scale flow so that it may be able to numerically predict the probable

occurrence of severe local storms and squall lines without calculating
individual convective circulations of small scale.

In the study by Sasaki in 1964, he pointed out that one of the im-
portant parameters which may correlate to the occurrence of severe
storms seems to be the upward moisture flux from the planetary boundary
layer into the free atmosphere. The basic idea for it is simple; the
larger the upward moisture flux, the greater the latent heat released
due to condensation of moisture. Condensation of moisture is the process
which produces energies essential for the formation and development of
severe storms.

From the theoretical viewpoint, it is always possible to solve the
hydrodynamical equations in finite difference forms if adequate initial
and boundary conditions are given. Also with the aid of high speed compu-
ter, the numerical weather prediction has become an operationally feasible
technique. But the existing operational model with grid distance of
381 kilometers as used by NMC, is too large in mesh length to effectively
forecast the occurrence of severe local storms.

In view of this point, a dynamical model for forecasting the moisture
is studied in this paper. The model which was basically used by Sasaki
in 1964 was applied with some modifications in addition to the increase
of the vertical resolution in the boundary layer where moisture is most
densely distributed. The significance of increased vertical resolution
to the increased accuracy of moisture forecast was emphasized also by
Sasaki, based on his previous results and was later supported by a series
of moisture analyses in the lower atmosphere.

Smagorinsky (1956), in his study of the numerical predictions of
precipitation amounts, pointed out the necessity of including effects

of release of latent heat. If these influences were not considered, the computed vertical velocities were underestimated in regions of condensation by as much as an order of magnitude. The amplifying effect has also been demonstrated by Danard (1966). He was able to show mathematically that the inclusion of latent heat liberation in the so-called ω-equation, would increase in the magnitudes of the computed vertical motions in a saturated region.

Since water vapor is added to the air mainly by evaporation from oceans, lakes, and rivers, the central and southern United States area receives the majority of its moisture supply from the Gulf of Mexico. A rather common weather pattern that exists prior to the formation of thunderstorms in this area is a situation where high pressure dominates the eastern United states letting moisture flow from the Gulf of Mexico into this area (Miller, 1967). According to Harris (1968), the evaporation from the Gulf of Mexico is, therefore, important in determining the amount of moisture transported vertically upward into the free atmosphere.

Reap, in 1968, developed a three dimensional trajectory model to forecast temperature and dew point. He then, applied it to the severe storm prediction. His verification statistics for 74 test cases during May-July 1968 indicated a significant improvement over the primitive equation model forecasts in the lowest 150 mb, where temperature and moisture distributions are crucial to severe storms development. As a further refinement of temperature and dew point forecasts in the future, he recommended that in addition to the necessary terrain specification, all available sea-surface temperature data be included into the thermo-dynamic equations to provide an estimate of the sensible heat flux and

evaporative moisture flux from the ocean surface. He also suggested that a suitable statistical evaluation of ship-reported dew points, coupled with existing upper air data, is needed to provide a first estimate of the vertical moisture profiles in as many levels as may be feasible over data-sparse oceanic regions.

This paper describes an attempt to incorporate the influences of evaporation from the Gulf of Mexico, and the released latent heat into a numerical prediction model. The effects of topography are taken care of by using the relative vertical coordinate which is defined as $z^* = z - H(x, y)$ with $H(x, y)$ the height from the ground and z positive upward in the conventional cartesian coordinate. The most important problem is then the prediction of the moisture field by numerical technique and its verification against the observed data.

Four versions of the model are discussed: Experiment 1 is the basis of the model which neglects topography, evaporation and latent heat release; Experiment 2 has no evaporation and no latent heat release, but accounts for topography, i.e., uses topographical coordinate; Experiment 3 adds the effects of evaporation but without latent heat release; Experiment 4 only accounts for topography and latent heat release but excludes evaporation effects.

The forecasts made for the above four experiments were the initial data on 0600CST, March 25, 1967. The computed 12-hrs. results are compared with observed data in terms of the specific humidity in gm kg^{-1} over the central U. S. areas including the Gulf of Mexico.

2.0 The Governing Equations

The set of equations which governs this dynamic forecasting model for Experiment 1 was described by Sasaki (1967) and Chen (1968). This set is comprised of the Navier-Stokes equations of motion written in a Cartesian (x, y, z, t) system, the equation of mass continuity under the incompressible assumptions, the moisture equation neglecting non-adiabatic effects, and the hydrostatic equation for constant air density in the layer. The equation of thermodynamics is not included in this experiment to avoid any diabatic processes for the sake of simplifying the problem. The governing equations are now stated below with the notations as defined in Table 1.

$$\frac{du}{dt} - fv = -\frac{\partial \pi}{\partial x} + \frac{\partial}{\partial z}\left(K(z)\frac{\partial u}{\partial z}\right) , \qquad (2.1)$$

$$\frac{dv}{dt} + fu = -\frac{\partial \pi}{\partial y} + \frac{\partial}{\partial z}\left(K(z)\frac{\partial v}{\partial z}\right) , \qquad (2.2)$$

$$\frac{\partial u}{\partial x} + \frac{\partial v}{\partial y} + \frac{\partial w}{\partial z} = 0 , \qquad (2.3)$$

$$\frac{dq}{dt} = 0 , \qquad (2.4)$$

$$dp = -\rho g dz , \qquad (2.5)$$

$$\pi = \frac{p}{\rho} , \text{ or } d\pi = -g dz , \qquad (2.6)$$

where $\quad \dfrac{d}{dt} = \dfrac{\partial}{\partial t} + u\dfrac{\partial}{\partial x} + v\dfrac{\partial}{\partial y} + w\dfrac{\partial}{\partial z} .$

Since the horizontal scale is much larger than the vertical scale, and we are concerned only with the planetary boundary layer, the second derivatives of x and y components in the right hand side of (2.1) and (2.2) are justified to be negligible in comparison with $\partial^2 u/\partial z^2$ and $\partial^2 v/\partial z^2$.

In (2.1) and (2.2), the vertical component of eddy coefficients is assumed to be a linear function of height with 10^4 c. g. s. at the lowest level at 200 m above the ground to 4.3 x 10^5 c. g. s. at top level at 1.4 km. The validity of that approximation is open to discussion. Baddley (1968) in his study of wind and temperature profile in the planetary boundary layer making use of data from an instrumented TV tower (WKY, Oklahoma City) showed that 10^4 c. g. s. would give a profile which closely approximated the observed wind for the lower levels of the tower, while 10^5 c. g. s. gave a close approximation to the observed wind for the upper level of the tower at 445 meters.

(2.4) is the continuity equation for moisture in its simplest form. Evaporation is discounted temporarily in this first experiment. The physical picture tries to see how the moisture is advected by the wind if the three-dimensional wind components were known. In the central U. S. region, the major supply of moisture is the advection of specific himidity from the Gulf of Mexico, particularly when a cold front associated with a low system, producing a strong southerly wind, is approaching Oklahoma.

Coriolis parameter, f, is assumed constant 8.365 x 10^{-5} sec^{-1}. Air density, ρ , is 1.08 x 10^{-3} gm cm^{-3}, and acceleration of gravity is assumed constant, 980 cm sec^{-2}.

The validity of this model for Experiment 1 was tested before a more sophisticated model was formulated for other experiments.

2.1 Modified Models for Experiments 2, 3, and 4

In these models, more physical properties are included. The general characteristics common to these models are four vertical levels; the primitive equations; a horizontal grid size of 165 kilometers

everywhere neglecting the map factor which is unity at 60 degrees
latitude.

The basic difference is the use of the topographical coordinate
in these models. The cartesian coordinate system is transferred into
the topographical coordinate system (x, y, z*, t) by defining the relative
vertical coordinate z* = z-H(x, y). As seen in Fig. 1, H(x, y) is the
ground elevation that is read from the geographical map (Fig. 2), and
smoothed before the integration to make the slope less than 1/750 in
order to avoid instability in the scheme (Appendix A). The thermodynamic
equation is added to describe the effect of evaporation and latent heat
release.

The x and y components of the Navier-Stokes, continuity, hydro-
dynamic, moisture, and thermodynamic equations derived in Appendix B,
using the relative vertical coordinate, are now stated below:

$$\frac{du}{dt} - fv = -\frac{\partial \pi}{\partial x} - g\frac{\partial H}{\partial x} + \frac{\partial}{\partial z}\left(K(z)\frac{\partial u}{\partial z}\right) , \tag{2.7}$$

$$\frac{dv}{dt} + fu = -\frac{\partial \pi}{\partial y} - g\frac{\partial H}{\partial y} + \frac{\partial}{\partial z}\left(K(z)\frac{\partial v}{\partial z}\right) , \tag{2.8}$$

$$\frac{\partial u}{\partial x} + \frac{\partial v}{\partial y} + \frac{\partial w^*}{\partial z} = 0 , \tag{2.9}$$

$$\pi = \frac{p}{\rho} , \quad dp = \frac{-pg}{RT} dz , \tag{2.10}$$

$$\frac{dq}{dt} = E , \tag{2.11}$$

$$\theta = T\left(\frac{1000}{p}\right)^{R/c_p} \tag{2.12}$$

$$\frac{d\theta}{dt} = \frac{\theta}{c_p T} Q , \tag{2.13}$$

where $w^* = w - u\frac{\partial H}{\partial x} - v\frac{\partial H}{\partial y}$ and $\frac{d}{dt} = \frac{\partial}{\partial t} + u\frac{\partial}{\partial x} + v\frac{\partial}{\partial y} + w^*\frac{\partial}{\partial z}$.

The above set of equations is distinctly different from the previous
set of governing equations used in the Experiment 1. In the equations
of motion, two terms with gravitational acceleration appear. These
terms are results of using the topographical coordinate, and may be
physically viewed as correction terms to the pressure field. As an
illustration, we may redefine a new pressure field as $\hat{\pi}$, which is mathe-
matically expressible as

$$\hat{\pi} = \frac{p}{\rho} + gH = \pi + gH \ .$$

By taking the partial derivative of the above expression in both x and y
directions respectively, $g\frac{\partial H}{\partial x}$ and $g\frac{\partial H}{\partial y}$ were obtained. It should be
mentioned here that these two terms may constitute a serious stability
problem, if not properly handled, as indicated by Kasahara and Washington
(1967), in their work on the global general circulation model.

(2.11) says that the change in specific humidity is only equal to
the gain due to evaporation which may be calculated by using Sverdrup's
(1951) formula from the sea surface. In mathematical expression, Sverdrup's
evaporation formula is given by $E = 3.7 \ (e_\omega - e_a) \ |V|$, where e_ω and
e_a denote respectively the vapor pressure at some height and at sea
surface. V is the wind speed. It is clear from the evaporation formula
that maximum evaporation should occur in areas of strong wind, warm water,
and cold air, as cold air over warm water will result in a large specific
humidity difference. Harris (1968) calculated evaporation and moisture
transport from the Gulf of Mexico utilizing the same set of data on 0600CST,
March 25, 1967. His result of evaporation output in the form of (qw)
at 200-meter level was incorporated directly into the model as the initial
evaporation input (Fig. 3). However, the evaporation is assumed to stay

constant through the entire forecasting period and enters the problem
only as a boundary condition at 200-meter level.

(2.13) is the thermodynamic equation which includes the change of
potential temperature due to the latent heat released by the rising moist
air. It has been long known that the amount of heat liberated in a verti-
cal unit column is proportional to the total convergence of moisture.
Furthermore, Smagorinsky (1956), in his study of numerical predictions
of precipitation amounts pointed out the necessity of including effects
of release of latent heat. If this influence were not considered,
the computed vertical velocities would be underestimated in regions of
condensation by as much as an order of magnitude. Ogura (1964) based
on his estimation of time scale between small and large scale motion,
assumed that the release of latent heat took place instantly through
most of the troposphere once the air parcel with typical vertical velocities
inside cumulonimbus clouds starts to ascend. He was able, by specifying
temperature at some levels, to write

$$\frac{\theta}{c_p T} Q = \eta \frac{\partial \theta}{\partial p} \omega \quad , \quad \text{if} \quad \omega < 0$$

$$= 0 \qquad , \quad \text{if} \quad \omega > 0 \quad .$$

The nondimensional proportionality constant η was roughly estimated
as 3 to 4 by giving typical values of $\frac{\partial \theta}{\partial p}$ and the mixing ratio of water
vapor at the top of the boundary layer. By applying Ogura's method,
(2.13) is rewritten as

$$\frac{d\theta}{dt} = \eta \frac{\partial \theta}{\partial z} w^* \quad \text{if} \quad w^* > 0 \quad ,$$

$$= 0 \qquad \text{if} \quad w^* < 0 \quad ,$$

or
$$\left(\frac{\theta}{c_p T}\right) Q = \eta \frac{\partial \theta}{\partial z} w^* \quad \text{if} \quad w^* > 0 \ ,$$

$$= 0 \qquad \qquad \text{if} \quad w^* < 0 \ .$$

The partition of latent heat release is not considered in this calculation.

2.2 Physical Layouts of Parameters and Boundary Conditions

As mentioned earlier, this is a four-level model, equally spaced in the vertical direction from lowest level at 200 meters to the highest level at 1400 meters. On the z^* coordinate, all meteorological parameters such as temperature, pressure, specific humidity, and horizontal velocity are assigned at 200 m, 600 m, 1000 m and 1400 m above the ground. The vertical velocity is assigned at the ground level and at 100 m, 400 m, 800 m, 1200 m and 1600 m above the ground as shown below. On the constant z^* surface, the horizontal grid system is shown in Fig. 4 which shows the coverage of the area and its grid system.

```
- - - - - - - - - - - - - - - -    upper boundary (w = 0)

_____    z₄ (u,v,p,q,T,θ)      (1.4 km)

- - - - - - - - - - - - - - - -    w₄

_____    z₃ (u,v,p,q,T,θ)      (1.0 km)

- - - - - - - - - - - - - - - -    w₃

_____    z₂ (u,v,p,q,T,θ)      (0.6 km)

- - - - - - - - - - - - - - - -    w₂

_____    z₁ (u,v,p,q,T,θ)      (0.2 km)

- - - - - - - - - - - - - - - -    w₁

_____    surface (w = 0)
/ / / / / / / / / / / / / / / /
```

The upper boundary is $w = 0$, levels z_4 (u,v,p,q,T,θ) (1.4 km), w_4, z_3 (u,v,p,q,T,θ) (1.0 km), w_3, z_2 (u,v,p,q,T,θ) (0.6 km), w_2, z_1 (u,v,p,q,T,θ) (0.2 km), w_1, surface $(w = 0)$.
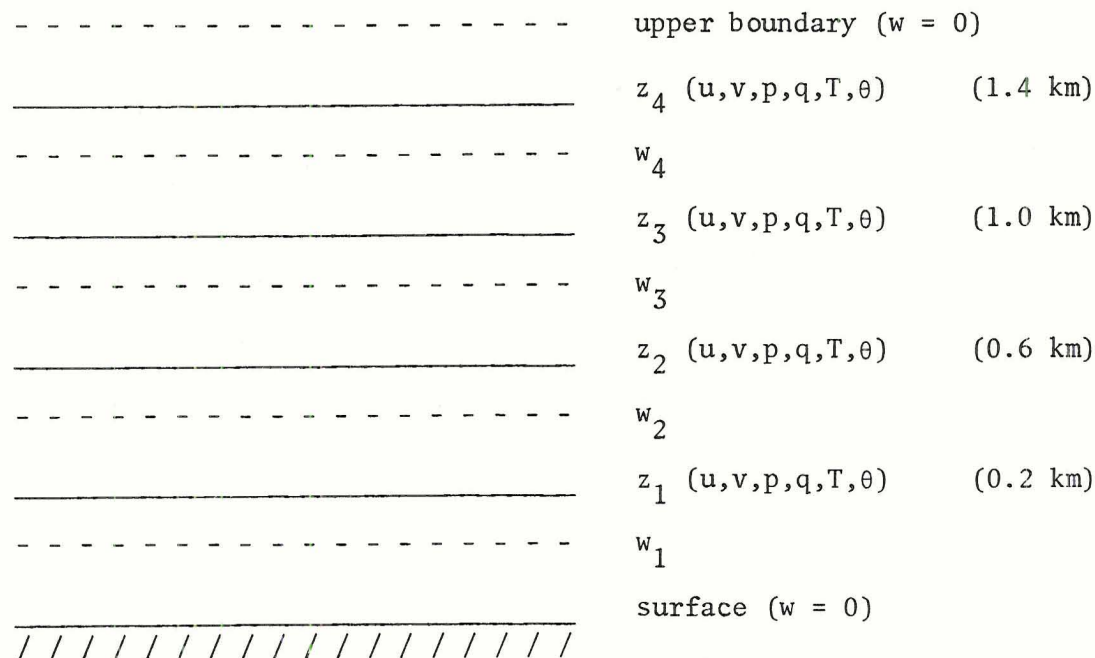
The vertical boundary conditions are chosen to be

$w = 0$ at surface, $w = 0$ at upper boundary.

In doing this, we are assuming that the upper boundary is rigid, thus allowing no momentum transfer above that boundary. This, of course, is not realistic and some other ideas such as incorporating the present operational NWP output of w into this model are suggested.

The lateral boundary conditions, which are usually more difficult to set up than the vertical boundary conditions, assume that the velocity profile is determined by the profile one grid point inward. Such boundary conditions are taken to smooth the velocity field at the lateral boundary at all levels to insure the stability of the scheme. Since we are dealing with a rather short integration period, the generated error waves do not invade the domain far from the boundary point, so we may treat the problem ignoring the effect of the finiteness of the domains (Matsuno, 1966).

3.0 Method of Solution

(2.1) to (2.6) provide the six equations with six dependent variables, u, v, w, π, p, q. Since ρ is constant, the set of equations and variables both reduce to five. The initial values of these parameters are given from the observation except the pressure field π , which is not obtained from the actual data but rather calculated from the wind field. Therefore, the calculation of the forecasted horizontal velocities in those equations cannot proceed until the pressure π is calculated for further use in (2.1) and (2.2).

From (2.3), the continuity equation is rewritten as

$$\frac{\partial w}{\partial z} = - \left(\frac{\partial u}{\partial x} + \frac{\partial v}{\partial y} \right) \quad .$$

By integrating over the height, it yields

$$\int_{z = 0}^{z = \text{upper boundary}} \frac{\partial w}{\partial z} \, dz = - \int_{z = 0}^{z = \text{upper boundary}} \left(\frac{\partial u}{\partial x} + \frac{\partial v}{\partial y} \right) dz \quad ,$$

$$w_{z = \text{upper boundary}} - w_{z = 0} = - \int_{z = 0}^{z = \text{upper boundary}} \left(\frac{\partial u}{\partial x} + \frac{\partial v}{\partial y} \right) dz \quad .$$

Assuming the following boundary conditions on the ground surface and at the top,

$$w_{z = 0} = 0 , \quad \text{and} \quad w_{z = \text{upper boundary}} = 0 \quad .$$

The integrated divergence is then required to be zero, i.e.,

$$\int_{z = 0}^{z = \text{upper boundary}} (\text{DIV } \vec{V}_h) \, dz = 0 , \tag{3.1}$$

where $\quad \text{DIV } \vec{V}_h \;=\; \dfrac{\partial u}{\partial x} \;+\; \dfrac{\partial v}{\partial y}\;.$

(3.1) describes the condition that has to be satisfied throughout all calculations.

The pressure field π in (2.1) and (2.2) is to be forecasted by the following method.

Let

u^1 be the u component neglecting the pressure gradient term, $-\dfrac{\partial \pi}{\partial x}$

v^1 be the v component neglecting the pressure gradient term, $-\dfrac{\partial \pi}{\partial y}$

then, the forecasted wind field is given by

$$u(t + \Delta t) \;=\; u'(t + \Delta t) + \zeta_x \;=\; u'(t + \Delta t) - \frac{\partial \pi}{\partial x}\,\Delta t \;,$$

$$v(t + \Delta t) \;=\; v'(t + \Delta t) + \zeta_y \;=\; v'(t + \Delta t) - \frac{\partial \pi}{\partial y}\,\Delta t \;.$$

By substituting the above equation into (3.1) they yield

$$\int_{z\,=\,0}^{z\,=\,\text{upper boundary}} \left[\frac{\partial u'}{\partial x}(t + \Delta t) + \frac{\partial v'}{\partial y}(t + \Delta t) - \frac{\partial^2 \pi}{\partial x^2}\,\Delta t - \frac{\partial^2 \pi}{\partial y^2}\,\Delta t \right] dz \;=\; 0 \;,$$

or

$$\int_{z\,=\,0}^{z\,=\,\text{upper boundary}} \left[\frac{\partial u'}{\partial x}(t + \Delta t) + \frac{\partial v'}{\partial y}(t + \Delta t) \right] dz \;=\; \int \left(\frac{\partial^2 \pi}{\partial x^2} + \frac{\partial^2 \pi}{\partial y^2} \right) \Delta t \; dz$$

i.e. $\quad \dfrac{\overline{\text{DIV } \vec{V}_h}}{\Delta t} \;=\; \overline{\nabla^2 \pi}\;.$ $\hfill$ (3.2)

The mean pressure field is then obtained by the relaxation method that is discussed in Section 4.0.

Once the mean pressure field is determined, the hydrostatic equation is used to solve for the pressure field at each level. Since we are interested in the motions whose horizontal dimension is much larger than the vertical one, the use of this approximation will be permitted.

From (2.6), the following algebraic equations are valid;

$$\pi_2 = \pi_1 - g\Delta z$$

$$\pi_3 = \pi_2 - g\Delta z$$

$$\pi_4 = \pi_3 - g\Delta z$$

By adding the above equations, it gives

$$\pi_1 + \pi_2 + \pi_3 + \pi_4 = 2\pi_1 + \pi_2 + \pi_3 - 3g\Delta z \ .$$

After algebraic manipulation, the above equality becomes

$$\pi_1 + \pi_2 + \pi_3 + \pi_4 = 4\pi_1 - 6g\Delta z \ .$$

or

$$\pi_1 = (\pi_1 + \pi_2 + \pi_3 + \pi_4)/4 + 6g\Delta z/4 = \tilde{\pi} + \frac{3}{2} g\Delta z \ .$$

Similarly,

$$\pi_2 = \tilde{\pi} + g\Delta z/2$$

$$\pi_3 = \tilde{\pi} - g\Delta z/2$$

$$\pi_4 = \tilde{\pi} - 3g\Delta z/2 \ .$$

(2.1) and (2.2) can be used to calculate u and v wind fields.

The vertical velocity w at each level is then computed from (2.3), which yields

$$w_z = - \int_{z=0}^{z} \left(\frac{\partial u}{\partial x} + \frac{\partial v}{\partial y} \right) dz \ .$$

At this point the specific humidity q in (2.4) can be computed from values of u, v, w, and initial values of q. The marching process is then repeated to proceed through time.

In the experiments 2, 3, and 4, the calculation of pressure is a little different. Because the topographical terms enter into the equations of motion, $g\nabla^2 H$ has to be added into the right hand side of (3.2). Otherwise, the same method applies to the Experiments 2, 3, and 4 except in the handling of hydrostatic equation where air density is no longer constant under these experiments.

From (2.10) we are able to write

$$
\begin{aligned}
p_2 &= p_1 \exp\left(-\frac{c}{\tilde{T}_{12}}\right) \\
p_3 &= p_2 \exp\left(-\frac{c}{\tilde{T}_{23}}\right) \\
p_4 &= p_3 \exp\left(-\frac{c}{\tilde{T}_{34}}\right)
\end{aligned}
\tag{3.3}
$$

where $c = g\Delta z/R$, R is the dry air constant, and $\tilde{T}_{ab}$ is the mean temperature between levels a and b. By adding the above expressions, we get

$$
\begin{aligned}
p_2 + p_3 + p_4 &= p_1 \exp\left(-\frac{c}{\tilde{T}_{12}}\right) + p_2 \exp\left(-\frac{c}{\tilde{T}_{23}}\right) + p_3 \exp\left(-\frac{c}{\tilde{T}_{34}}\right) \\
&= p_1 \exp\left(-\frac{c}{\tilde{T}_{12}}\right) + p_1 \exp\left(-\frac{c}{\tilde{T}_{12}}\right) \exp\left(-\frac{c}{\tilde{T}_{23}}\right) \\
&\quad + p_1 \exp\left(-\frac{c}{\tilde{T}_{12}}\right) \exp\left(-\frac{c}{\tilde{T}_{23}}\right) \exp\left(-\frac{c}{\tilde{T}_{34}}\right) \quad .
\end{aligned}
$$

Now $\qquad 4\tilde{p} = p_1 + p_2 + p_3 + p_4$

$$= p_1 \left[1 + \exp\left(- \frac{c}{\tilde{T}_{12}}\right) + \exp\left(- \frac{c}{\tilde{T}_{12}}\right) \exp\left(- \frac{c}{\tilde{T}_{23}}\right) \right.$$
$$\left. + \exp\left(- \frac{c}{\tilde{T}_{12}}\right) \exp\left(- \frac{c}{\tilde{T}_{23}}\right) \exp\left(- \frac{c}{\tilde{T}_{34}}\right) \right] .$$

therefore,

$$p_1 = 4\tilde{p} / \left[1 + \exp\left(- \frac{c}{\tilde{T}_{12}}\right) + \exp\left(- \frac{c}{\tilde{T}_{12}}\right) \exp\left(- \frac{c}{\tilde{T}_{23}}\right) \right.$$
$$\left. + \exp\left(- \frac{c}{\tilde{T}_{12}}\right) \exp\left(- \frac{c}{\tilde{T}_{23}}\right) \exp\left(- \frac{c}{\tilde{T}_{34}}\right) \right] .$$

Once p_1 is determined, p_2, p_3 and p_4 are solved by (3.3).

3.1 Data Analysis

In order to test the model and make a forecast, the real data was used. Advantage was taken of the data already extracted by French (1968), and to make the results of his study more easily adaptable to the prediction model. He obtained the original weather data from the University of Texas. It consisted of the upper air data and surface observations for all stations in the United States, and the Northern Hemisphere surface and 700 mb charts. The data used was valid for each twelve hour period beginning with 1800 CST, 24 March 1967 and ending 1800 CST, 25 March 1967. Sea surface temperature data was obtained from Texas A & M University for the period 25 March to 1 April, 1967.

Temperature, dew point, pressure, wind speed, and direction were plotted at levels 200 meters apart. From the soundings temperature and dew point were selected for each 200-meter level, and by assuming the

mixing ratio equal to the specific humidity, the specific humidity at
each level was obtained. Since wind direction and speed were plotted
at each 1000 ft. on the soundings, it was easy to interpolate the values
for each 200 meter level.

Interpolation of pressure for each 200 meters was essentially
done by using the following hydrostatic equations,

$$\frac{\ln p - \ln 850}{z - z(850)} = \frac{\ln 1000 - \ln 850}{z(1000) - z(850)} \,,$$

and

$$\frac{\ln p - \ln 700}{z - z(700)} = \frac{\ln 850 - \ln 700}{z(850) - z(700)} \,.$$

In the above equations, z was the desired level in meters. All
other parameters were available from three standard levels of the sounding
at 1000, 850 and 700 mb.

Due to the unavailability of upper air data over Mexico and the
Gulf of Mexico, the data from the Northern Hemisphere surface and 700
mb charts was interpolated to obtain data in these areas. It is there-
fore expected that this data may not be as accurate as it would be if
the entire sounding was available. The measure of evaporation from the
Gulf of Mexico is obtained from the results of Harris's work. The
surface water temperature of the Gulf is based on the data obtained
from ship measurements which were made by the staff of the Texas A & M
University for the period 25 March - 1 April 1967. From this temperature,
the saturated specific humidity is calculated and assumed unchanged
throughout the period of forecast.

After all the data was analyzed for each 200 meters, topography was considered in order to change all parameters from (x, y, z) to (x, y, z*) coordinate. This was done by computer.

3.2 Initialization of Data -- Objective Analysis

The most important thing to obtain a satisfactory result in the numerical computation of hydrodynamical equations is the initialization of data coupled with an energy conserved mathematical scheme. To perform a time integration of hydrodynamical equations, the initial conditions are needed for the geopotential, wind, vertical velocity, temperature, and moisture if thermodynamics is included. These conditions can, in priniciple, be obtained from the observed data. However, the data may not always be used directly as initial conditions, even though the forecasting domain is covered with a dense observing network. If the data is used directly, a short-period oscillation of motion is produced (Miyakoda and Moyer, 1968). This is partly due to inaccurracy in the data and to the incompleteness of the forecasting model.

In view of this fact, an objective analysis on the data is needed to filter out or to suppress unnecessary meteorological high frequency noises contained in the initial data. The classical technique is solving the balance equation by assuming the fluid is in a state such that its flow is always adjusted to the pressure field under the control of gravity and coriolis force.

The method applied in this analysis is rather straight forward. Taking the observed u and v components of wind data, the vorticity is computed. The streamfunction ψ is then obtained by solving the Poisson equation, $\zeta = \nabla^2 \psi$, where ζ is relative vorticity. The non-divergent

wind is recalculated by using

$$u = - \frac{\partial \psi}{\partial y} \quad , \qquad \text{and} \qquad v = \frac{\partial \psi}{\partial x} \quad .$$

Note that this is satisfied by (2.3) as zero initial vertical velocity is assumed, although this is not a realistic assumption.

Initialization is a subject of urgent importance. In 1965, Smagorinsky et al. made two forecasts with his primitive equation model, one with a certain value of initial vertical velocity and the other with zero initial vertical velocity, showed similar results for at least 5 days. There is, however, a possibility that the solutions would begin to depart from each other after 5 days. Recently, an interesting initialization method was proposed by Miyakoda and Moyer (1968). Their method uses the geopotential as the only input. Sasaki (1968) made one step forward on the initialization problems by using all available data, not only geopotential but also wind, etc., to develop a dynamical objective analysis scheme to get the initial values which were able to suppress unnecessary high frequency modes to an adequate level. The initial values thus obtained by his method may not fully satisfy the so called "balance" condition but do not contain high frequency modes unnecessary for the short range forecast.

4.0 The Numerical Model

(2.1) through (2.6) as well as (2.7) through (2.13) of Section 2.0
are used to forecast the moisture under various physical assumptions.
Although these primitive equations have the advantage of being easier
to incorporate various physical effects into the model, it is neverthe-
less, impossible to get analytical solutions due to their high degree
of non-linearity. A practical solution to this problem is the method
of finite-difference approximations.

The governing equations are approximated in finite-difference form
using the modified Lax-Wendroff scheme as discussed by Richtmyer (1962)
to evaluate the derivatives. A 10-minute time step is used along with
the horizontal grid distance of 165 kilometers in order to satisfy the
computational stability requirement (Appendix C) of the system.

4.1 The Finite-Difference Equations

As mentioned in the previous section, a stable calculation scheme
is required to get a meaningful prediction results when the prognostic
equations are integrated. The simplest forward-time step method of
solution is subject to computational instability when the centered
space difference is used. This means that the numerical solutions will
begin to show a characteristic structure in which the motion degenerates
into eddies of a few grid intervals in size and results in an inability
of the finite grid to properly resolve them. The eddies, once formed,
usually intensify without limit, causing computational instability and
explosive growth of the total kinetic energy of the system. Moreover,
it is also observed in the past that as integration proceeds the energy

is distributed over a broader and broader range of wave number. For a shorter period forecast, the stability is not a serious problem, but for a long-term integration of the hydrodynamical equations, it is necessary to overcome the computational instability through a proper and delicate computational design of the integration, because the non-linear instability has its origin in space-truncated errors. Because of these difficulties, there are some criterion as to the choices of time increment in relation to the grid distance and also the eddy coefficient such that the high frequency waves will be damped off and a stable solution will, therefore, be quaranteed. Lax-Wendroff scheme satisfies this desired characteristic and has been successfully used in short-period forecasting problems in meteorology.

Corresponding to (2.1), (2.2) and (2.4), the finite-difference equations, applicable to the (i, j, k)-th grid point (exclusive of the boundary points) and the n-th time steps are as follows:

$$
U^*_{n+1} (i,j,k) = \frac{1}{4} (U_n(i+1, j, k) + U_n(i-1, j, k) + U_n(i, j+1, k)
$$

$$
+ U_n(i, j-1, k)) - \Delta t U_n(i,j,k)\nabla_x U_n - \Delta t V_n(i,j,k)\nabla g U_n
$$

$$
- \Delta t w_n(i,j,k)\nabla_z U_n + \Delta t f V_n(i,j,k) - \Delta t \nabla_x \pi_n
$$

$$
+ K(z)\nabla_z\nabla_z U_n \quad , \tag{4.1}
$$

$$
V^*_{n+1} (i,j,k) = \frac{1}{4} (V_n(i+1, J, k) + V_n(i-1, j, k) + V_n(i, j+1, k)
$$

$$
+ V_n(i, j-1, k)) - \Delta t U_n(i,j,k)\nabla_x V_n - \Delta t V_n(i,j,k)\nabla_y V_n
$$

$$
- \Delta t w_n(i,j,k)\nabla_z V_n - \Delta t f U_n(i,j,k) - \Delta t \nabla_y \pi_n
$$

$$
+ K(z)\nabla_z\nabla_z V_n \quad , \tag{4.2}
$$

$$q^*_{n+1}(i,j,k) = \frac{1}{4}(q_n(i+1, j, k) + q_n(i-1, j, k) + q_n(i, j+1, k)$$

$$+ q_n(i, j-1, k) - \Delta t U_n(i,j,k) \nabla_x q_n - \Delta t V_n(i,j,k) \nabla_y q_n$$

$$- \Delta t w_n(i,j,k) \nabla_z q_n \quad , \tag{4.3}$$

$$U_{n+1}(i,j,k) = U_n(i,j,k) - \Delta t U^*_{n+1}(i,j,k) \nabla_x U^*_{n+1} - \Delta t V^*_{n+1}(i,j,k) \nabla_y U^*_{n+1}$$

$$- \Delta t w_n(i,j,k) \nabla_z U^*_{n+1} + \Delta t f V^*_{n+1}(i,j,k) - \Delta t \nabla_x \pi_n$$

$$+ K(z) \nabla_z \nabla_z U^*_{n+1} \quad , \tag{4.4}$$

$$V_{n+1}(i,j,k) = V_n(i,j,k) - \Delta t U^*_{n+1}(i,j,k) \nabla_x V^*_{n+1} - \Delta t V^*_{n+1}(i,j,k) \nabla_y V^*_{n+1}$$

$$- \Delta t w_n(i,j,k) \nabla_z V^*_{n+1} - \Delta t f U^*_{n+1}(i,j,k) - \Delta t \nabla_y \pi_n$$

$$+ K(z) \nabla_z \nabla_z V^*_{n+1} \quad , \tag{4.5}$$

$$q_{n+1}(i,j,k) = q_n(i,j,k) - \Delta t U_{n+1}(i,j,k) \nabla_x q^*_{n+1}$$

$$- \Delta t V_{n+1}(i,j,k) \nabla_y q^*_{n+1} - \Delta t w_{n+1}(i,j,k) \nabla_z q^*_{n+1} \quad , \tag{4.6}$$

with i, j = 2, 3, . . . M-1, k = 1, . . . 4, and n = 1, 2, 3, . . .

The finite difference operator is defined as

$$\nabla_x U_n = \frac{U_n(i+1, j, k) - U_n(i-1, j, k)}{2\Delta x}$$

$$\nabla_y U_n = \frac{U_n(i, j+1, k) - U_n(i, j-1, k)}{2\Delta y}$$

$$\nabla_z U_n = \frac{U_n(i, j, k+1) - U_n(i, j, k-1)}{2\Delta z}$$

and $\qquad \nabla_z \nabla_z U_n = \dfrac{U_n(i, j, K+1) + U_n(i, j, k-1) - 2U_n(i, j, k)}{(\Delta z)^2} \qquad .$

The last two expressions in the vertical derivatives are bound by the conditions that any quanity such as $U_n(i, j, k+1)$, or $U_n(i, j, k-1)$ has to be zero respectively at $k = 4$, and 1.

All space derivatives in (4.1) through (4.6) are approximated by centered space differences. In the vertical boundaries at levels 1 and 4, the forward and backward space differences were first tried separately in hopes of yielding more valid approximations at those boundaries. But it turned out that instability developed and finally, the centered-space difference had to be used. The consistency of the space derivatives in finite approximations is important in order to avoid instability.

The diagnostic equations such as equation of continuity are simply approximated by centered-space difference. In the calculation of vertical velocity, the horizontal wind components from (4.4) and (4.5) are used to compute horizontal divergence, and the trapezoidal rule is applied to integrate the calculated horizontal divergence up to the desired height to obtain the vertical velocity.

The vertical velocity, w, and pressure field, π, are calculated only once at each time step as noticed from (4.1) through (4.5). Unlike these two parameters, u and v components as well as specific humidity q are calculated twice at each time step as shown in the equations. The pressure terms in (4.1) and (4.2) are actually calculated by the method already described in the previous sections.

As pointed out earlier, in solving for pressure field at each single level, the mean pressure is obtained from numerical solution of (3.2). The technique for solving this Poisson equation is by applying the so-called extrapolated Liebman relaxation method. The idea in general,

is giving the initial values on the boundary and also the general values in the entire domain of the region and then by successive approximations, it generates an ordered sequence of approximations, each one better than the previous one. In this method, with a good choice of relaxation parameter, which usually lies between 1 and 2, can produce dramatic savings in the computing time to converge to the desired values. In this study the relaxation parameter is given as 1.68, and it took less than 30 iterations to converge to the desired values. The number of iterations required, of course, depends on the limitation of the chosen converging criterion.

After pressure field and vertical velocity have been determined at each grid point, (4.1) through (4.6) are applied mechanically to obtain forecasted wind components and specific humidity. The finite-difference models for Experiments 2, 3, and 4 are treated the same way except the thermodynamic equation is added to account for the potential temperature changes.

5.0 Results and Discussion

5.1 Synoptic Discussion

The synoptic situation chosen for this study is a rather common weather pattern that exists prior to the formation of thunderstorms in the central United States (Miller, 1967). High pressure dominated the east-central U. S., allowing moisture flow from the Gulf of Mexico into Texas and northward to the Great Plains. At the surface a cold front was moving slowly into the northwest corner of the grid beginning at 1800 CST on 24 May 1967. The front extended across the extreme north-west corner of the grid area from Omaha, Nebraska to central Colorado (Fig. 5). A squall line had developed in western Oklahoma and severe storm activity was occurring in the extreme southern states. Empirically we know that the moisture which helped produce this severe weather came from the Gulf of Mexico.

From the sounding at 0600 CST, 25 March 1967 (Fig. 6), an area of maximum specific humidity of 14 gm km^{-1} at the 200 meter MSL was located at the Gulf area. With increasing height, the area of high moisture concentration elongated from the Gulf of Mexico into central Texas. 10 gm kg^{-1} maximum was observed at the 1000 meter level. At 1800 meters, the moisture maximum of 8 gm kg^{-1} was completely shifted inland into North Texas and South Oklahoma. The whole pattern at this level was fairly homogeneous with only 2 gm kg^{-1} difference between the south and north part of the grid. The distribution of the observed moisture patterns suggests that it would be desirable to have higher vertical resolution in the lower part of the boundary layer.

5.2 Experiment 1, The Basic Model

This is the basic experiment of the model without using topo-
graphical coordinate, evaporation, and liberation of latent heat.
All parameters were obtained by interpolation and assigned to each
constant height level above the ground.

The forecasted moisture (Fig. 7) displayed two systematic moisture
tongues; one extending from the southeast part of the Gulf of Mexico
north-westward into Oklahoma; the other extending from Colorado through
New Mexico into Texas. The maximum moisture concentration was 14 gm kg^{-1},
and was centered in Southern Louisiana and part of the Gulf of Mexico.
It is interesting to note that the largest gradient of moisture was
located near the area where the flow pattern seemed to converge (Fig. 8).
A dry line, separating the warm humid air from the Gulf of Mexico and
cooler drier air from northwest was the direct result of this big gradient.
This area corresponds to great instability with Showalter index of -3
(Fig. 9). Furthermore, the observed low was centered just south of
the Oklahoma panhandle with the cold front behind the dry line. All
these constitute a favorable condition for storm formation. The
observed weather at this time did show a very long band of squall line
(Fig. 11) with light storms. Along Texas, Oklahoma, Missouri, Arkansas,
and part of Kansas some slight rain showers were also observed in the
south and east Texas.

Another interesting feature was the orientation of the moisture
tongue which showed a substantial tilting of its ridge line toward
the left as compared with the initial distribution (Fig. 10). This
phenomenon was pointed out by Dr. R. Inman of NSSL (personal communica-
tion), and further elaboration on this will be investigated. However,

it is suspected that under some particular synoptic situations, some mechanism may produce an organized distribution of moisture within a short period. The tilting of the moisture tongue is significant in the severe storms forecasting problem, since by knowing the axis of tilting, it would serve to better locate the probable locations of severe storms.

Due to the non-availability of reliable data at higher topographical areas, the forecasted pressure indicated a relatively poor agreement both in pattern and magnitude. To forecast the pressure, the mean value of pressure at four levels on the boundary was taken to solve Poisson's equation. It is, therefore, conceivable that the accurate initail pressure data on the boundary will improve the result.

The forecasted moisture was verified against the observed value (Fig. 12) at 1800 CST, 25 March 1967. The major error was found in the Gulf area with 3 gm kg^{-1} higher than the observed value (Fig. 13). This may have to do with the accuracy of sea surface temperature measurement. Another error with 2 gm kg^{-1} across Oklahoma, Arkansas and Tennessee is expected to be removed when more physics is considered in the following experiments.

5.3 Experiment 2, Effects of Topography

Surface roughness is the major factor which causes convergence or divergence in the planetary boundary layer. In regions of sloping terrain, the air immediately above the surface is subjected to forced vertical motion. As a result, the moisture distribution should be expected to have close correlation with vertical velocity caused by topography.

Results of Experiment 1 indicated that the moisture forecast without using the topographical coordinate was about 3 gm kg^{-1} too high in the region of the Gulf of Mexico as compared with the observed pattern. This forecasted error is reduced as expected when utilizing the topographical coordinate accounting for surface roughness.

Figure 14 is the result of Experiment 2. The major difference when compared with Experiment 1 is shown in the western boundary of the grid where the topography is relatively high. The general pattern is similar otherwise, except the 14 gm kg^{-1} line is now completely situated in the Gulf area. Figure 15 shows the difference between forecasted and observed values of moisture on the z* coordinate. Note that significant improvement is made over the eastern boundary. Most of the errors are still centered in the Gulf area as in the case of Experiment 1. Over the land two places with error of 2 gm kg^{-1} were indicated respectively at Northern Georgia and Mexico. These errors are most likely due to inadequate data in the higher topographical areas.

The forecasted patterns of (wq) are shown In Fig. 16. The value of q is at 1 km and w is the linear average of the values at 0.8 and 1 km. The forecasted patterns indicated a rather elongated distribution of (wq) from the southwest boundary of the grid along the northern coast line of the Gulf of Mexico to the northeast boundary of the grid. The elongated belt was changing steadily for the first 6-hour forecasted period. At the end of six hours, a significant increase in the southwest U. S. is observed. Furthermore, the pattern of (wq) developed into a more solid belt from the southwest corner along the Gulf coast into the northeast end corner of the boundary. The forecasted location of the belt agrees favorably with the observed squall lines and also compared well with the

observed Showalter index which is shown in Fig. 9. The forecasted

vertical velocity, w, at 1000 meters is shown in Fig. 17. Note that

the major upward motion is in the southwest part of Texas and southern

Oklahoma where the cold front is propagating slowly eastward.

5.4 Experiment 3, Effect of Evaporation

Experiment 2 showed that the topography is an important considera-

tion in getting a better moisture forecast. In this experiment, evapora-

tion from the Gulf of Mexico as a constant moisture source is added to

the model to investigate the effect of evaporation to the moisture

distribution inland within a 12-hour period.

The general pattern in Fig. 18 is similar to that of Experiment 2.

However, the whole pattern is seen shifted inland from the south particularly

in the middle eastern portion of the forecasted domain. The line of

14 gm kg^{-1} situated in the south of Florida peninsula in Experiment 2

is now moving inland to the edge of the coast line. No significant

change is observed in the western portion. This phenomenon corresponds

fairly well with the satellite photographs (Fig. 19), that shows a wide

band of clouds extending from the eastern Gulf along the Appalachian

mountains at 1938 z, March 26, 1967. Although the forecasted time is

19 hours earlier than the satellite photographic time, it was possible

from the forecasted distribution of moisture to show the development of

that cloud system.

Two locations with maximum magnitude of 17 gm kg^{-1} are shown in the

Gulf of Mexico area; one in the western part of the Gulf, and the other

one in the eastern part. These two areas correspond to the same locations

where the vertical moisture tranport was in maximum according to Harris

(1968). The western center of maximum vertical moisture transport is due

primarily to the convergence of horizontal moisture tranport in that

area, whereas the eastern center is a result of the large evaporation

that is occurring in the region.

Figure 20 is the difference in specific humidity between Experiment

2 and Experiment 3. There were two centers of maximum difference

contributed by evaporation from the Gulf of Mexico; one in the west with

3 gm kg^{-1}, the other is in the east with 3.5 gm kg^{-1}. Notice that the

location of the maximum difference in the eastern part of the Gulf

corresponds relatively well with that of maximum center as seen in Fig.

18, whereas the other center in the west has been shifted substantially

inland by northeast direction due to relatively strong horizontal

moisture transport in the latter area as shown in Fig. 22.

Figure 21 is the difference between the results of Experiment 3

and observed values of moisture. Over the land in the middle west the

forecasted value was very satisfactory, but over the Florida peninsula

the error was high. This augmented error over that area is mostly due

to constant source of evaporation that was assumed constant over the fore-

casted period. This is unrealistic. Therefore, some better observations

are necessary to improve the forecasting result.

The evaporation effects under the ordinary Cartesian coordinates

without topography are also made comparable to Fig. 20. This is shown

in Fig. 23 which has similar distribution in the moisture pattern regard-

less of topography.

The forecasted pattern of (wq) is shown in Fig. 24 which shows exactly

the same pattern as Fig. 16 at 1800 CST, except in the Gulf region where

(wq) is elongated due to evaporation from that area.

5.5 Experiment 4, Effects of Latent Heat Release

The evaporation, utilizing Harris's data is omitted temporarily to check the effect of latent heat release in the model. Figure 25 shows the result of Experiment 4. Significant reduction of maximum moisture in the eastern Gulf area is found, although the overall distribution still looks similar to that of Fig. 18. Figure 26 is the verification that shows the difference between Experiment 4 and the observed specific humidity at the same time. Note that improvement is made over the Gulf area, especially in the eastern boundary when compared with Fig. 21. Note also that the 2 gm kg^{-1} line appeared in the eastern boundary in Fig. 15 is now shifted closer towards the boundary. This is undoubtedly the most satisfactory forecasted result among various experiments performed in regard to the moisture forecast utilizing this particular set of initial data.

Another interesting result in this experiment is the pattern of (wq) which is shown in Fig. 27. A very strong and systemized belt is indicated in the southwestern Texas area. This location corresponds fairly well with the observed squall line location. This is a big improvement in the forecast of squall line formation taking accounts of latent heat release. Figure 28 shows the forecasted vertical velocity at 1000 meters above the ground. The strongest upward motion forecasted at the southwestern Texas location corresponds better with the Showalter index as compared with the w, forecasted by Experiment 2 (Fig. 17).

To understand how much moisture is being added into the local station within 12 hours, a constant tracking of moisture at 1 hour interval is made for three stations as shown in Fig. 29. Oklahoma City shows a predicted, steady inflow of moisture from initial values of 8.0 t0 10.1 gm kg^{-1},

a net increase of 2.1 gm kg^{-1} over the 12-hour period. A satellite

photograph taken at 1247 CST, March 25, 1967 (Fig. 30) showing a wide

band of clouds extending from western Gulf into Oklahoma seems in

excellent agreement with this predicted result. The second station,

Amarillo, Texas, which is approximately 1 kilometer above MSL showed

a very slight gain of moisture for the first 8 hours, then goes steady

at 6.5 gm kg^{-1} for a 2-hour period. At the end of 10 hours, the moisture

starts decreasing! The surface map, (Fig. 5) at 1800 CST, March 25,

1967 showed at map time the cold front had already passed the station.

So the air behind the station is cooler and drier. This is a very good

example justifying why the predicted moisture at that station is decreas-

ing two hours before map time. Another station, Nashville, Tennessee,

showed a very steady gain of moisture with only 0.7 gm kg^{-1} over 12

hours forecasted period. This station has relatively less moisture influx

from the Gulf of Mexico due to its overwhelming east wind from the western

Atlantic area. Furthermore, the air from the Atlantic dries out after

crossing the Appalachian Mountains. The verification of forecasted

moisture at 1 kilometer is also shown in Fig. 31. The error is only

found in the Gulf of Mexico. Very satisfactory forecast result is ob-

tained in the central U. S. area.

Additional physical effect such as evaporation from the Gulf of

Mexico is again included into Experiment 4 to check the forecasted results.

It turns out, as shown in Fig. 32, that the general feature is still

not much improved when compared with Fig. 21 which is the verification

of Experiment 3.

The constant tracking of moisture at three stations were performed

in order to see the evaporation effect. At Oklahoma City (Fig. 33), the

amount of moisture added due to evaporation is not discernible until 10

hours later. A total net increase of 0.4 gm kg^{-1} within 12 hours due to evaporation is forecasted at Oklahoma City. At Amarillo, Texas, the effect of evaporation is perfectly zero. This is indicated explicitly by the northeast wind direction at that station. At Nashville, Tennessee, evaporation effect is very strong. This station shows its sign of evaporation effect at 6 hours later and ends up with a net gain of 0.8 gm kg^{-1} within 12 hours. A shorter distance from the center of maximum evaporation rate (Fig. 34) is the reason.

In Experiment 3, the error of forecasted moisture in the Gulf area is assumed due partly to the evaporation data used in that area which is too large. In anticipation of correction that error, only half of the calculated evaporation data was taken to be incorporated with the effect of latent heat release in the model. Figure 35 is the verification of this experiment. Major errors with 2 gm kg^{-1} are confined to the Gulf area and in the eastern boundary of the grid. A good forecast was observed throughout the rest of the forecasted area.

5.6 Water Content

To check the validity of this model in its ability to forecast the amount of precipitable water in a vertical column of air, the average specific humidity in the layer is multiplied by the height difference between two layers and then multiplied again by the air density, to obtain the precipitable water. The mathematical expression is given by

$$W = \int_{z_1}^{z_2} \rho q \, dz = \rho \int_{z_1}^{z_2} q \, dz$$

where W is liquid water in gm cm^{-2}, ρ is air denisty assuming

constant, and q is specific humidity in gm kg^{-1}.

Figure 36 shows the forecasted precipitable water in gm cm^{-2} con-

tained in a vertical column from lower boundary at 200 meters up to the

upper boundary at 1400 meters. The maximum value spreads from the Gulf

area with 1.3 gm cm^{-2} northward through Louisiana and southern Arkansas

to 1.2 gm cm^{-2} at the southwestern boundary of Oklahoma State. The

surface map reproduced from the Washington Daily weather map (Fig. 37)

at 1200 CST, March 25, 1967 showed at map time, which is 6 hours earlier

than the verified time, that there were two shaded areas in eastern

Oklahoma and the whole state of Louisiana where precipitation was occurring.

The forecasted areas of maximum precipitable water were actually moved

considerably further east when compared with Fig. 37. In this particular

case, an excellent correlation does exist between the forecasted maximum

precipitable water and the observed precipitation area.

Figure 38 is the verification showing the difference between the

forecasted precipitable water and the observed values at 1800 CST,

March 25, 1967. Most of the errors with 0.2 gm cm^{-2} are located in the

Gulf areas. In land, the Appalachian Mountains are the only shallow place

with errors of 0.2 gm cm^{-2}. A good feasibility in this model for render-

ing adequate moisture forecast seems established.

6.0 Conclusions

This study has covered discussions of four numerical experiments:
(1) the simplest model without using topographical coordinates, (2) the
topographical effects (3) the effects of evaporation from the Gulf of
Mexico, and (4) the effects of latent heat release.

The storm index, wq, computed at 1 kilometer, was also tested to
prove the validity of this forecasting model in verifying against the
observed weather conditions. The final forecast was accomplished by
computing the precipitable water from forecasted specific humidity at
each level. The precipitable water forecasts were also verified against
observed data. The error fields, compiled using this verification
method, counted only the algebraic error at the 200 meter level above
the ground.

Direct evaluation of the error field showed that the 12-hour pre-
diction of moisture by this model appeared to be adequate. Of course, it
is difficult to generalize the results simply based on the limited exper-
iment from a single synoptic case. However, this study has provided a
good basis for a further extension of its work, and could eventually
develop into an operational model supplement to the present NMC model.

The significant results were these:

1. The moisture ridge lines or the moisture tongue showed a good
correspondence in location between forecasted and observed values in all
experiments, at the 200 meter-level above the ground.

2. The ridge line of the forecasted 12-hour moisture pattern had
displayed a tendency to tilt toward the west in this particular synoptic
situation, as compared with the initial observed values. The degree of
tilting, depends, very closely, on the speed of movement of the cold front.

3. Forecasted moisture in the central U. S. proved to be very satisfactory, but in the eastern U. S. along the Appalachian Mountains the error was about 2 gm kg^{-1}. This error occurred in all experiments. Correction should be made when more reliable data are available.

4. The storm index, defined as wq, successfully described the squall line position when topographical and liberation of latent heats were accounted for in the model.

5. For the 12-hour forecast in the central U. S. region, the latent heat release seemed to be more important than the evaporation effect. Since evaporation from central Gulf of Mexico only affected coastal states (Fig. 20) under moderate wind speeds, say 6 m sec^{-1}.

6. Good agreement was also observed between the forecasted moisture gradients and the existing instability lines.

7. It was possible to detect the passage of a cold front by a constant tracking of the moisture at a specific station as was shown in Fig. 28.

8. The forecasted precipitable water in Experiment 4 agreed fairly well with the observed value, except in the Gulf area and the Appalachian Mountains. Furthermore, the forecasted location of maximum precipitable water also corresponded well to the observed precipitation areas, although there was no positive statistical correlation between the two.

Evaluation of verifications revealed that the improvement in the forecasted results were made in the higher levels such as at the 1-km level. Also, the forecasted error was smallest in the relatively flat part of the grid areas. Due to terrain elevation, missing data had to be entered for many grid points at the lower levels. The amount of

missing data decreased with the higher levels which contributed to better forecast results there.

From the theoretical viewpoint, this study has made an effort to consider a major factor, evaporation, in a model and to prove this model is feasible in short-range forecasting even under the unrealistic assumption of constant evaporation throughout the entire forecast period. At the present time, there is no better way of treating the evaporation and specific humidity based on the observational frequency in the Gulf area, because of the lack of upper air data from reporting stations in Mexico and around the Gulf of Mexico. For a longer period forecast such as 24 hours or more, the evaporation from the Gulf of Mexico is apparently decisive in deteriming the development of severe storms in the central U. S. Under such circumstances, the diurnal variation of temperature is no longer negligible if effective evaporation is to be considered.

The vertical velocity field calculated by this model was comparable only to the magnitude of the synoptic scale even when latent heat release was accounted for. This may be due partly to the fact that the solution at 12 hours, attained by this model, is still undergoing initial adjustment, and partly due to the unrealistic assumption of zero vertical velocity at the upper boundary. It is proposed that the output of w from the NMC operational model be incorporated into the present model as the initial vertical velocity field so that more accurate results could be expected.

Another error of w may occur from the inaccuracy of initial horizontal wind components. As we pointed out earlier, the nondivergent wind does not reflect the actual wind. For one thing, the nondivergent

wind tends to lose too much meteorological information which is usually important for local short-range forecasts, particularly around the frontal areas and low level jets. For a short-range forecast, these characteristics are not favorable, and should be removed by applying Sasaki's objective analysis (1968) method, using all available data.

A logical extension of this study should put more emphasis on the vertical resolution of moisture in the boundary layer. It is strongly believed that the vertical resolution is the major factor which influences the differences in forecast result rather than the initial vertical field for the short-range forecast. Because, contrary to the vertical behavior of temperature patterns with height, the moisture pattern shows a pronounced tendency to vary, especially in the lowest 1.5 km or so. We cannot rely on the distribution of moisture or relative humidity at the surface for the patterns aloft particularly in the Gulf areas.

More synoptic cases would have to be tested in order to finalize the feasibility of this numerical model on an operational basis.

BIBLIOGRAPHY

Arakawa, A., 1966: Computational design for long-term numerical integration of the equation of fluid motion: two-dimensional incompressible flow. Part 1. J. Meteor. Phys., Vol. 1, No. 1, 119-143.

Aubert, E. F., 1957: On the release of latent heat as a factor in large scale atmospheric motions. J. Meteor., 14, 527 - 542.

Baddley, H. M., 1968: Investigation of wind and temperature profiles in the planetary boundary layer. Master's Thesis, University of Oklahoma, 54 pp.

Chen, T. S., 1968: A study of numerical moisture forecast. University of Oklahoma, ARL-1653-7, ESSA. E22-108-68(G), 21 pp.

Danard, M. B., 1966: A quasi-geostrophic numerical model incorporating effects of release of latent heat. J. Appl. Meteor., Vol. 5, 1, 85-93.

French, L. R., 1968: Forecast of the lower troposphere in relation to severe local storms. Master's Thesis, University of Oklahoma, 64 pp.

Harris, J. E., 1968: Evaporation and moisture transport from the Gulf of Mexico. Master's Thesis, University of Oklahoma, 41 pp.

Kasahara, A., and W. M. Washington, 1967: NCAR global circulation model of the atmosphere. Mon. Wea. Rev., Vol. 95, No. 7, 389-402.

Matsuno, T., 1966: Numerical integration of the primitive equations by a simulated backward difference method. J. Meteor. Soc. Japan, 11 Vol. 44, 1, 76-84.

_____, 1966: False reflection of waves at the boundary due to the use of finite difference. J. Meteor. Soc. Japan, 11, Vol. 44, 2, 145-157.

McCracken, D., and W. S. Dorn, 1964: Numerical methods and Fortran programming with applications in engineering and science. New York, John Wiley and Sons, Inc., 457 pp.

Miller, R. C., 1967: Notes on analysis and severe storm forecasting procedures of the Military Weather Warning Center. Air Weather Service Tech., Report No. 200.

Miyakoda, K., and R. W. Moyer, 1968: A method of initialization for dynamical weather forecasting. Tellus, 20, 113-128.

Ogura, Y., 1964: Frictionally controlled, thermally driven circulations in a circular vortex with application to tropical cyclones. J. Atmos. Sci., 21, 610-621.

Ooyama, K., 1963: A dynamical model for the study of tropical cyclone development. Dept. of Meteor. and Oceanography, New York University, 26 pp.

Priestley, C. H., 1959: Turbulent transfer in the lower atmosphere. The University of Chicago Press, 130 pp.

Reap, R. M., 1968: Prediction of temperature and dew point by three-dimensional trajectories. ESSA Tech. memorandum, WBTM TDL 15, 20 pp.

Richtmyer, R. D., 1962: A survey of difference methods for non-steady fluid dynamics. NCAR Tech. Notes, 63-2, 26 pp.

Sasaki, Y., 1967: Dynamical forecasting of severe local storms. Pre-liminary Report, Bulletin Amer. Meteor. Soc., 495 pp.

_____, et al., 1967: Dynamical forecasting of severe local storms. Final Report, University of Oklahoma Research Grant, ESSA E22-56-67(N), 13 pp.

_____, 1968: Numerical variational method of objective analysis; principle of initialization. Report No. 10, University of Okla-homa, 21 pp.

Smagorinsky, J., 1956: On the inclusion of moist adiabatic processes in numerical prediction models. Ber D. Deutsches Wetterd., 5, No. 38, 82-90.

_____, 1965: Prediction experiment with 9-level general circulation model. Proceedings of the international symposium on dynamics of large scale processis in the atmosphere, Moscow, U.S.S.R., 23-30 June 1965.

Stackpole, J. D., 1968: Operational prediction model at the National Meteorological Center. U. S. Dept. of Commerce, ESSA, 34 pp.

Sverdrup, H. U., 1937: On the evaporations from the oceans. J. Marine Res., Vol. 1, 3-14.

_____, 1951: Evaporation from the oceans. Compendium of Meteorology, 1071-1081.

Syono, S., and M. Yamasaki, 1966: Stability of symmetrical motions driven by latent heat release by cumulus convection under the existence of surface friction. J. Meteor. Soc. Japan, 11, Vol. 44, 6, 353-375.

Thompson, P. D., 1961: Numerical weather analysis and predictions. The MacMillan Co., New York, 170 pp.

APPENDIX A

Criterion of Smoothing Topography

Since this term $g\frac{\partial H}{\partial x}$ arises when the topographical coordinate is applied in the x-component of the equation of motion, this term has to be, at most, equal to or less than the other terms in the equation in its order of magnitude in order to prevent amplification of predicted wind field due to too much contribution from the topographical gradient. For a crude estimation, the following approximation is valid for the x-component of the equation of motion.

$$\frac{\partial u}{\partial t} \sim - g \frac{\partial H}{\partial x} \quad . \tag{A-1}$$

Rewriting in difference form, (A-1) becomes

$$U^{n+1} \sim U^n - \Delta t \; g \; \frac{\Delta H}{\Delta x} \tag{A-2}$$

Assuming U^{n+1} and U^n have the same order of magnitude (A-2) is non-dimentionalized by dividing through U^n to yield

$$1 \sim 1 - \frac{\Delta t g}{U^n} \; \frac{\Delta H}{\Delta x} \tag{A-3}$$

The constraint to (A-3) is $\left| \frac{\Delta t g}{U^n} \; \frac{\Delta H}{\Delta x} \right|$ has to be smaller than or, at most, equal to unity to satisfy the stability, i.e.,

$$\frac{\Delta t g}{U^n} \frac{\Delta H}{\Delta x} < 1 \; , \quad \text{or} \quad \frac{\Delta H}{\Delta x} < \frac{U^n}{\Delta t g} \quad .$$

By choosing Δt = 10 minutes, and U^n = 8 m sec^{-1}, gravity acceleration, g = 980 cm sec^{-2}, the topographical gradient becomes

$$\frac{\Delta H}{\Delta x} < \frac{8 \times 10^2}{600 \times 980} = \frac{1}{735} \quad .$$

If allowing for smaller values of U^n in the lower levels, as is the usual case, the following inequality,

$$\frac{\Delta H}{\Delta x} < \frac{1}{750}$$

should insure stable solutions.

APPENDIX B

Derivation of Governing Differential Equations in

Orographic Coordinates

The derivation of the set of differential equations governing this model using orographic coordinates was performed by Sasaki in 1967. The coordinate system is so called a relative cartesian system. The positive x-axis is eastward along the local parallel, the positive y-axis is northward along the local meridion, and the positive z*-axis is perpendicular to a level surface above the constant height, H(x, y), measured from the ground.

As defined earlier in the text, z* = z - H(x, y). Where z represents the vertical coordinate in the ordinary cartesian system, and H(x, y) is the topographical height from the ground. The transformation of z into z*, based on the above relations between two vertical coordinates, is given below.

$$
\left.\frac{\partial}{\partial x}\right)_z = \left.\frac{\partial}{\partial x}\right)_{z^*} + \frac{\partial z^*}{\partial x}\frac{\partial}{\partial z^*} = \left.\frac{\partial}{\partial x}\right)_{z^*} - \frac{\partial H}{\partial x}\frac{\partial}{\partial z^*} \tag{B-1}
$$

$$
\left.\frac{\partial}{\partial y}\right)_z = \left.\frac{\partial}{\partial y}\right)_{z^*} + \frac{\partial z^*}{\partial y}\frac{\partial}{\partial z^*} = \left.\frac{\partial}{\partial y}\right)_{z^*} - \frac{\partial H}{\partial y}\frac{\partial}{\partial z^*} \tag{B-2}
$$

$$
\frac{\partial}{\partial z} = \frac{\partial}{\partial z^*} \tag{B-3}
$$

Using the above relations, the equation of motion in the x-component in the z coordinate, i.e.,

$$
\frac{\partial u}{\partial t} + u\frac{\partial u}{\partial x} + v\frac{\partial u}{\partial y} + w\frac{\partial u}{\partial z} - fv = -\frac{\partial \pi}{\partial x} + \frac{\partial}{\partial z}\left(K(z)\frac{\partial u}{\partial z}\right)
$$

is ready to be transformed into the following expression,

$$\frac{\partial u}{\partial t}\Bigg\}_{z*} + u\frac{\partial u}{\partial x}\Bigg\}_{z*} - u\frac{\partial H}{\partial x}\frac{\partial u}{\partial z*} + v\frac{\partial u}{\partial y}\Bigg\}_{z*} - v\frac{\partial H}{\partial y}\frac{\partial u}{\partial z*} + w\frac{\partial u}{\partial z*}$$

$$-fv = -\frac{\partial \pi}{\partial x}\Bigg\}_{z*} + \frac{\partial H}{\partial x}\frac{\partial \pi}{\partial z*} + \frac{\partial}{\partial z*}\left(K(z*)\frac{\partial u}{\partial z*}\right) \quad . \qquad (B-4)$$

(B-4) is rearranged to become

$$\frac{\partial u}{\partial t}\Bigg\}_{z*} + u\frac{\partial u}{\partial x}\Bigg\}_{z*} + v\frac{\partial u}{\partial y}\Bigg\}_{z*} + \left(w - u\frac{\partial H}{\partial x} - v\frac{\partial H}{\partial y}\right)\frac{\partial u}{\partial z*}$$

$$-fv = -\frac{\partial \pi}{\partial x}\Bigg\}_{z*} - g\frac{\partial H}{\partial x}\Bigg\}_{z*} + \frac{\partial}{\partial z*}\left(K(z*)\frac{\partial u}{\partial z*}\right) \quad . \qquad (B-5)$$

By defining $w* = w - u\frac{\partial H}{\partial x} - v\frac{\partial H}{\partial y}$, and drops all other superscripts *,
(B-5) is rewritten as

$$\frac{\partial u}{\partial t} + u\frac{\partial u}{\partial x} + v\frac{\partial u}{\partial y} + \omega*\frac{\partial u}{\partial z} - fv$$

$$= -\frac{\partial \pi}{\partial x} - g\frac{\partial H}{\partial x} + \frac{\partial}{\partial z}\left(K(z)\frac{\partial u}{\partial z}\right) \quad .$$

Using the expressions in (B-1) through (B-3) and following the algebraic manipulation as demonstrated above, the governing equations from (2.7) through (2.13) in Section 2.0 were obtained.

APPENDIX C

Investigation of Computational Stability

The modified Lax-Wendroff scheme for the system of differential equation of

$$\frac{\partial u}{\partial t} + A \frac{\partial u}{\partial x} = K \frac{\partial^2 u}{\partial x^2}$$

is

$$U_j^{n+1} = U_j^n - \frac{\Delta t A}{2 \Delta x} (U_{j+1}^n - U_{j-1}^n) + \frac{1}{2} \left(\frac{\Delta t}{\Delta x} \right)^2 A^2 (U_{j+1}^n - 2U_j^n + U_{j-1}^n)$$

$$+ \frac{\Delta t K}{(\Delta x)^2} (U_{j+1}^n + U_{j-1}^n - 2U_j^n), \qquad (C-1)$$

where

A = constant,

K = coefficient of eddy viscosity,

Δx = grid distantce,

U = wind component along x axis,

Δt = time increment,

$n = \frac{t}{\Delta t}$, or $t = n\Delta t$.

Introducing the amplification factor which is defined as

$$G = \frac{u_j^{n+1}}{U_j^n} \quad , \quad U_j^n = U_0 e^{ikx} \quad , \qquad (C-2)$$

where

U_0 = constant ,

$x = j\Delta x$,

k = wave number ,

$i = \sqrt{-1}$.

Substituting (C-2) into (C-1) yields

$$G = 1 - \frac{i\Delta tA}{\Delta x} \left(\frac{e^{ik\Delta x} - e^{-ik\Delta x}}{2i} \right) + \left(\frac{\Delta t}{\Delta x} \right)^2 A^2 \left(\frac{e^{ik\Delta x} + e^{-ik\Delta x}}{2} \right)$$

$$- \left(\frac{\Delta t}{\Delta x} \right)^2 A^2 + \frac{2\Delta tK}{(\Delta x)^2} \left(\frac{e^{ik\Delta x} + e^{-ik\Delta x}}{2} \right) - \frac{2\Delta tK}{(\Delta x)^2}$$

$$= 1 - \frac{i\Delta tA}{\Delta x} \sin k\Delta t + \left(\frac{\Delta t}{\Delta x} \right)^2 A^2 \cos k\Delta x - \left(\frac{\Delta t}{\Delta x} \right)^2 A^2$$

$$+ \frac{2\Delta tK}{(\Delta x)^2} \cos k\Delta x - \frac{2\Delta tK}{(\Delta x)^2}$$

$$= 1 + \left(\frac{\Delta t}{\Delta x} \right)^2 A^2 (\cos k\Delta x - 1) + \frac{2\Delta tK}{(\Delta x)^2} (\cos k\Delta x - 1)$$

$$- \frac{i\Delta tA}{\Delta x} \sin k\Delta x$$

$$= 1 - (1 - \cos k\Delta x) \left[\frac{2\Delta tK}{(\Delta x)^2} + \left(\frac{\Delta t}{\Delta x} \right)^2 A^2 \right] - \frac{i\Delta tA}{\Delta x} \sin k\Delta x .$$

The condition for stability calls for G not to exceed 1 in absolute value.

Therefore,

$$\left[1 - (1 - \cos k\Delta x) \left(\frac{2\Delta tK}{(\Delta x)^2} + \left(\frac{\Delta t}{\Delta x} \right)^2 A^2 \right) \right]^2 + \left(\frac{\Delta tA}{\Delta x} \right)^2 \sin^2 k\Delta x \leq 1 .$$

For $k\Delta x = 0$, $1 \geq 1 \geq -1$,

for $k\Delta x = 90°$,

$$1 \geq \left[1 - \left(\frac{2\Delta tK}{(\Delta x)^2} + \left(\frac{\Delta tA}{\Delta x} \right)^2 \right) \right]^2 + \left(\frac{\Delta tA}{\Delta x} \right)^2 \geq -1 , \qquad (C-3)$$

If choosing particularly for

$$\frac{K\Delta t}{(\Delta x)^2} \leq \tfrac{1}{2} , \quad \text{and} \quad \frac{\Delta tA}{\Delta x} \leq \tfrac{1}{2} ,$$

Eq. (C-3) is satisfied.

Assuming the average wind speed below 2 km is 25 m sec^{-1}, the speed of a gravity wave is 100 m sec^{-1}, and grid distance, Δx, to be 165 km, then

$$\Delta t \leq \frac{\Delta x}{2(A+\bar{u})} = \frac{0.165 \times 10^8}{2 \times 12.5 \times 10^3} = 660 \text{ sec.}$$

For convenience, the time step increment is chosen as $\Delta t = 10$ min $= 600$ sec.

The maximum limit for K is determined from the relation constrained by

$$\frac{K\Delta t}{(\Delta x)^2} \leq \tfrac{1}{2} ,$$

or

$$K \leq \frac{(\Delta x)^2}{2(\Delta t)} = \frac{(0.165 \times 10^8)^2}{2 \times 600} = 22 \times 10^{10} \text{ c.g.s.}$$

So the eddy viscosity coefficient has to be less than or equal to 22×10^{10} c.g.s.

Table 1

Nomenclature

Note: An asterisk means the parameters are in relative vertical coordinate, unless stated otherwise.

E   Evaporation rate in gm cm^{-2} day^{-1} .

e   vapor pressure

f   Coriolis parameter equals to twice the angular velocity of the earth times the sine of the latitude.

g   Acceleration due to gravity.

H   Topographical height from the ground.

k   Eddy coefficient in cm^2 sec^{-1}.

p   Actual pressure of atmosphere.

q   specific humidity in gm kg^{-1}.

Q   Heating rate per unit mass.

R   Gas constant for dry air.

T   Absolute air temperature.

t   time in seconds.

Δt Time increment for numerical solution.

u   Eastward (x) component of wind velocity.

v   Northward (y) component of wind velocity.

w   Vertical (z) component of wind velocity.

W   Precipitable water in gm cm^{-2}.

x,y,z   Coordinate axis along eastward, northward, and vertical directions respectively.

$\Delta x, \Delta y, \Delta z$ Mesh sizes for numerical solutions in x,y,z components respectively.

π Air pressure divided by air density.

$\tilde{\pi}$ Average value of π in the layers.

θ Potential temperature.

c_p Specific heat capacity of dry air at constant pressure.

ρ Air density.

η Nondimensional proportionality constant.

ζ Relative vorticity.

ω Vertical velocity in pressure coordinate.

ψ Streamfunction in the x - y plane.

∇^2 Laplacian operator.
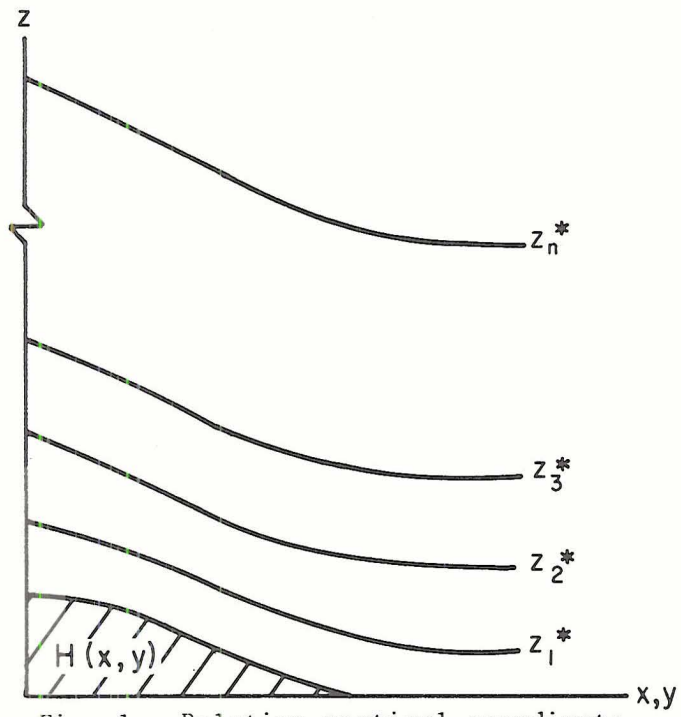
Fig. 1.   Relative vertical coordinate

Fig. 2. Topography
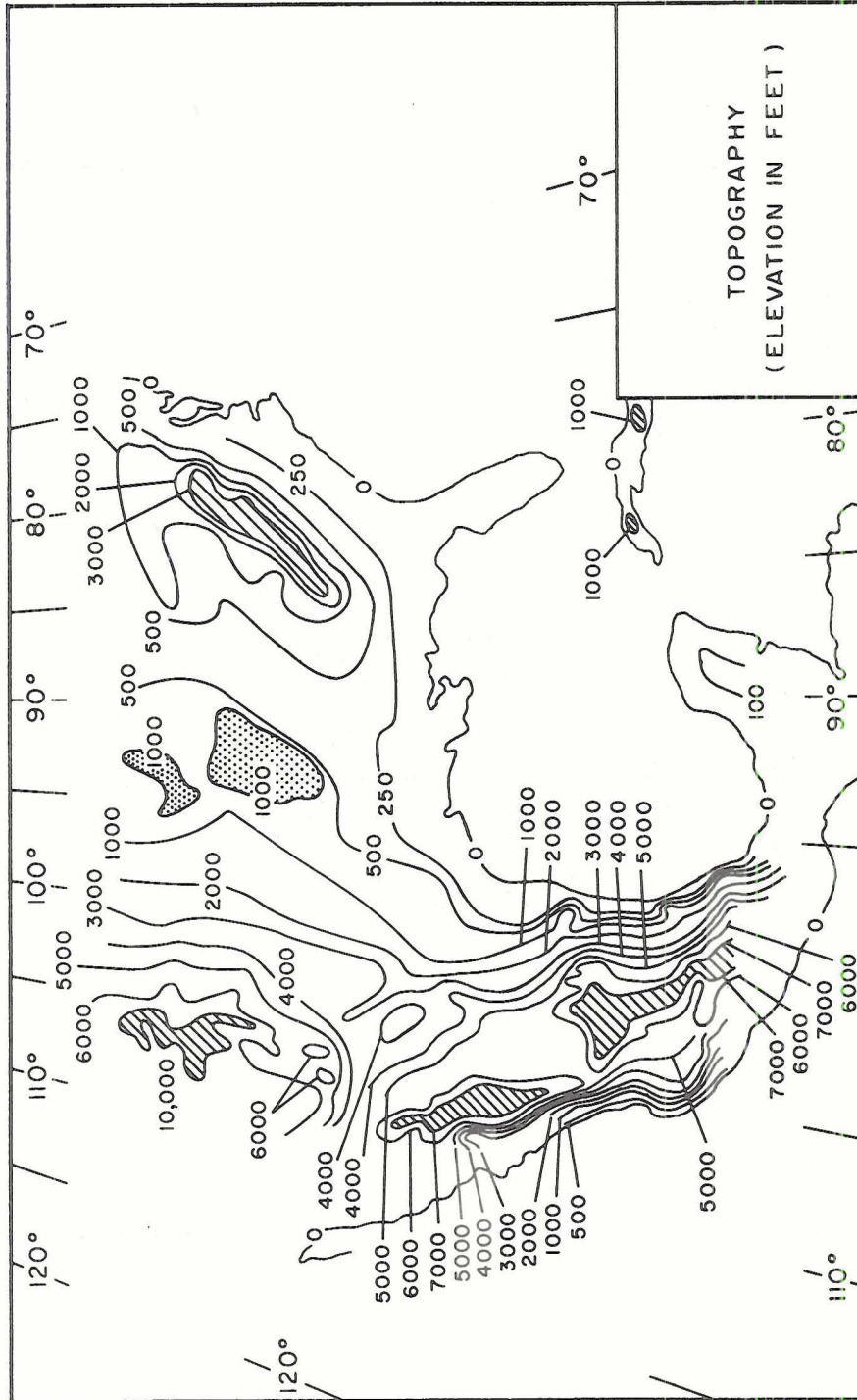
TOPOGRAPHY
(ELEVATION IN FEET)
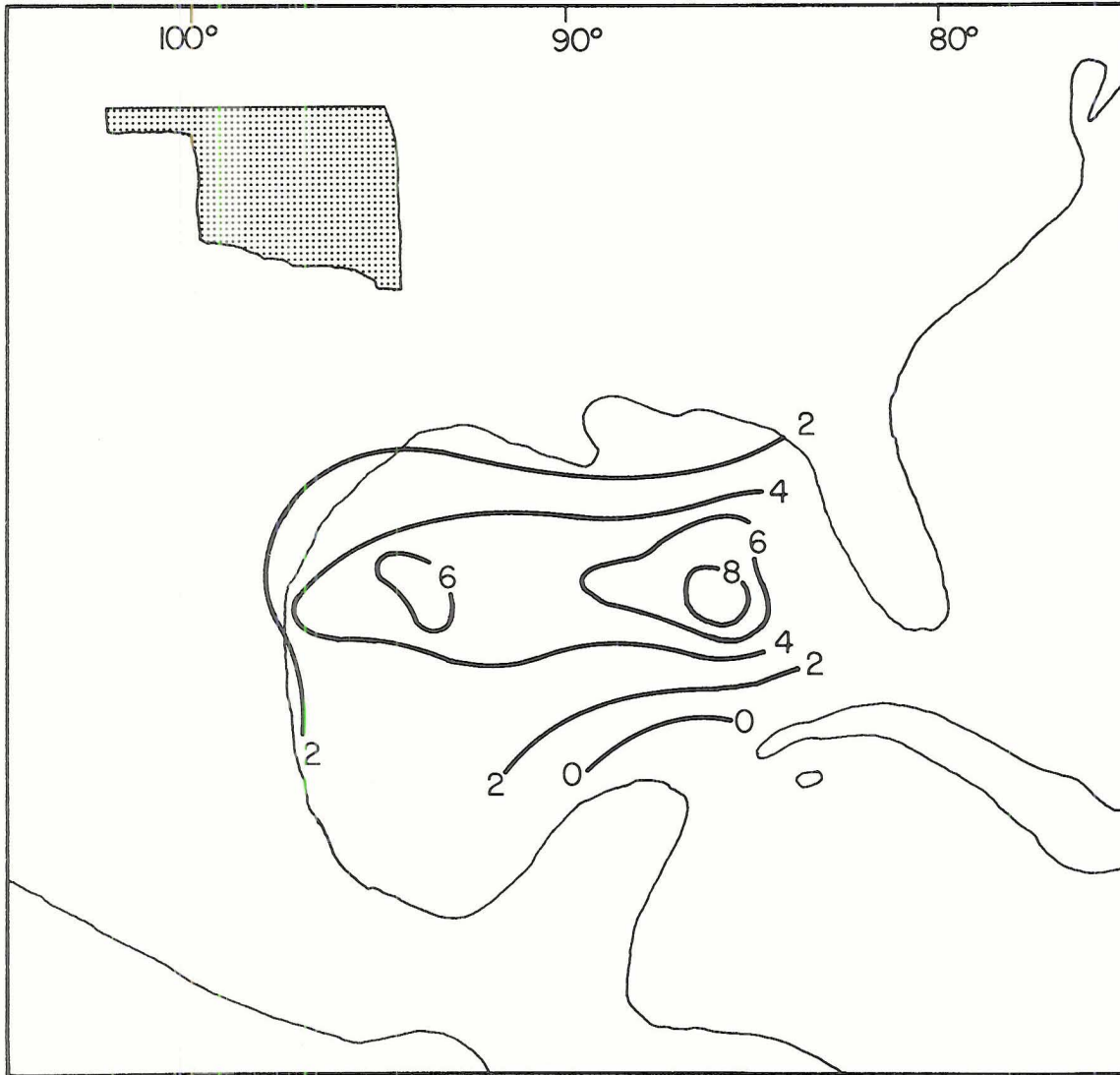
Fig. 3.   Vertical moisture transport qw (gm kg^{-1} cm sec^{-1}) at 200 meters.
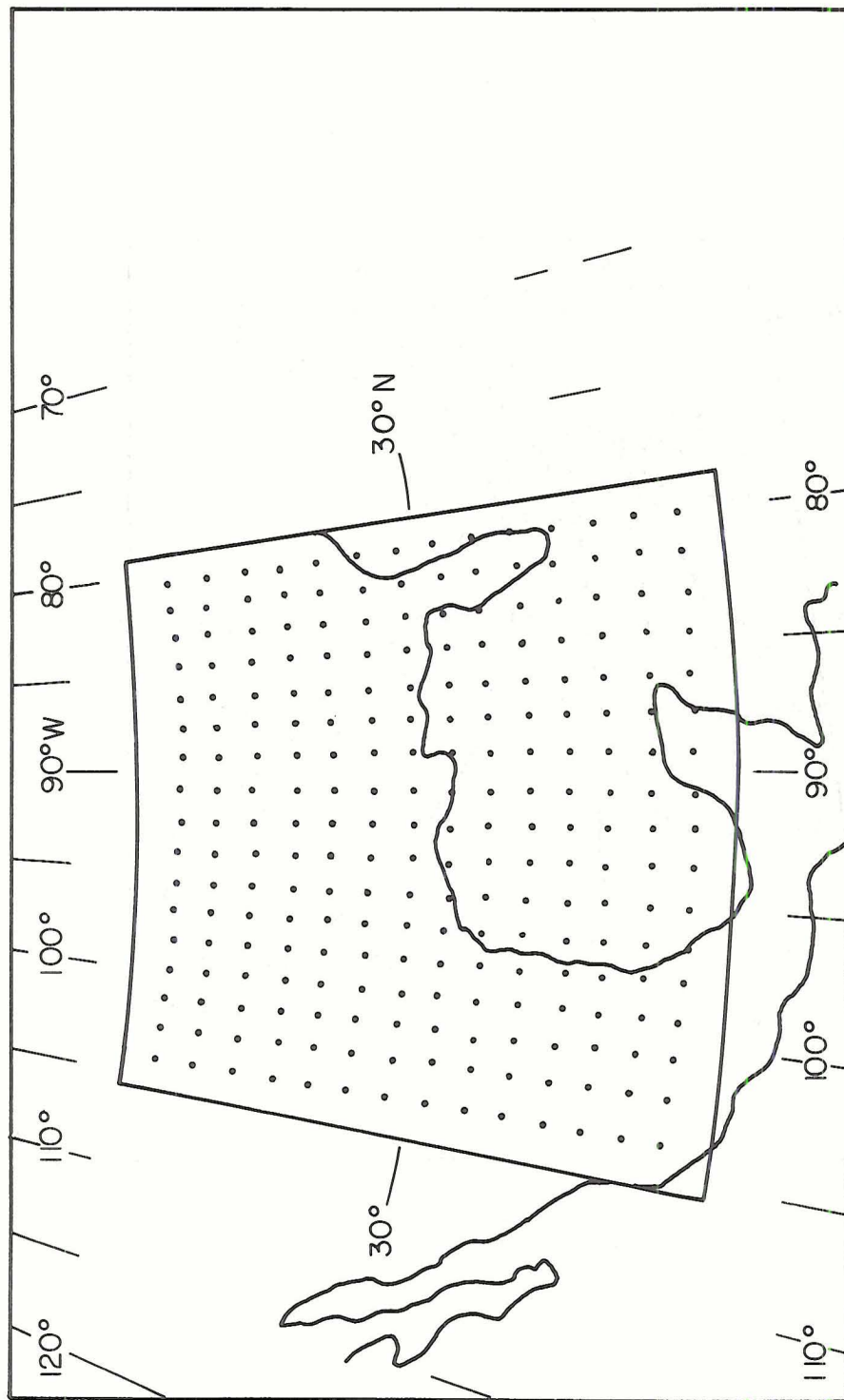
Fig. 4. Grid system
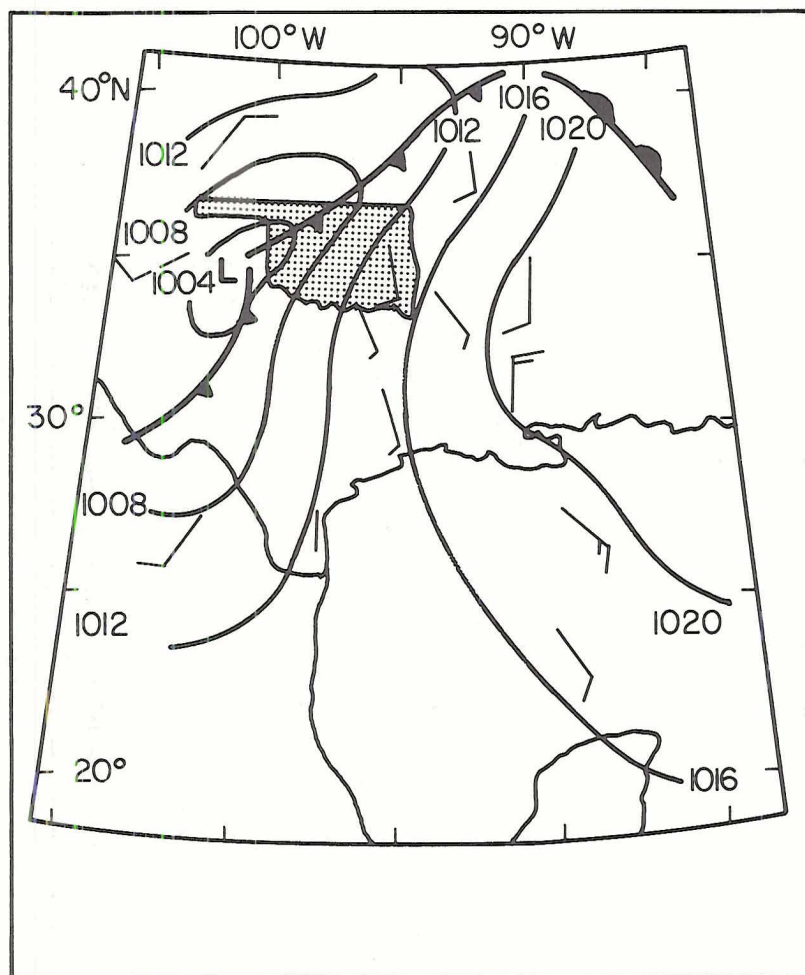
Fig. 5. Synoptic situation at 1800 CST, 25 March 1967. Isobars are 4 mb apart. Long wind barb is 10 kt.
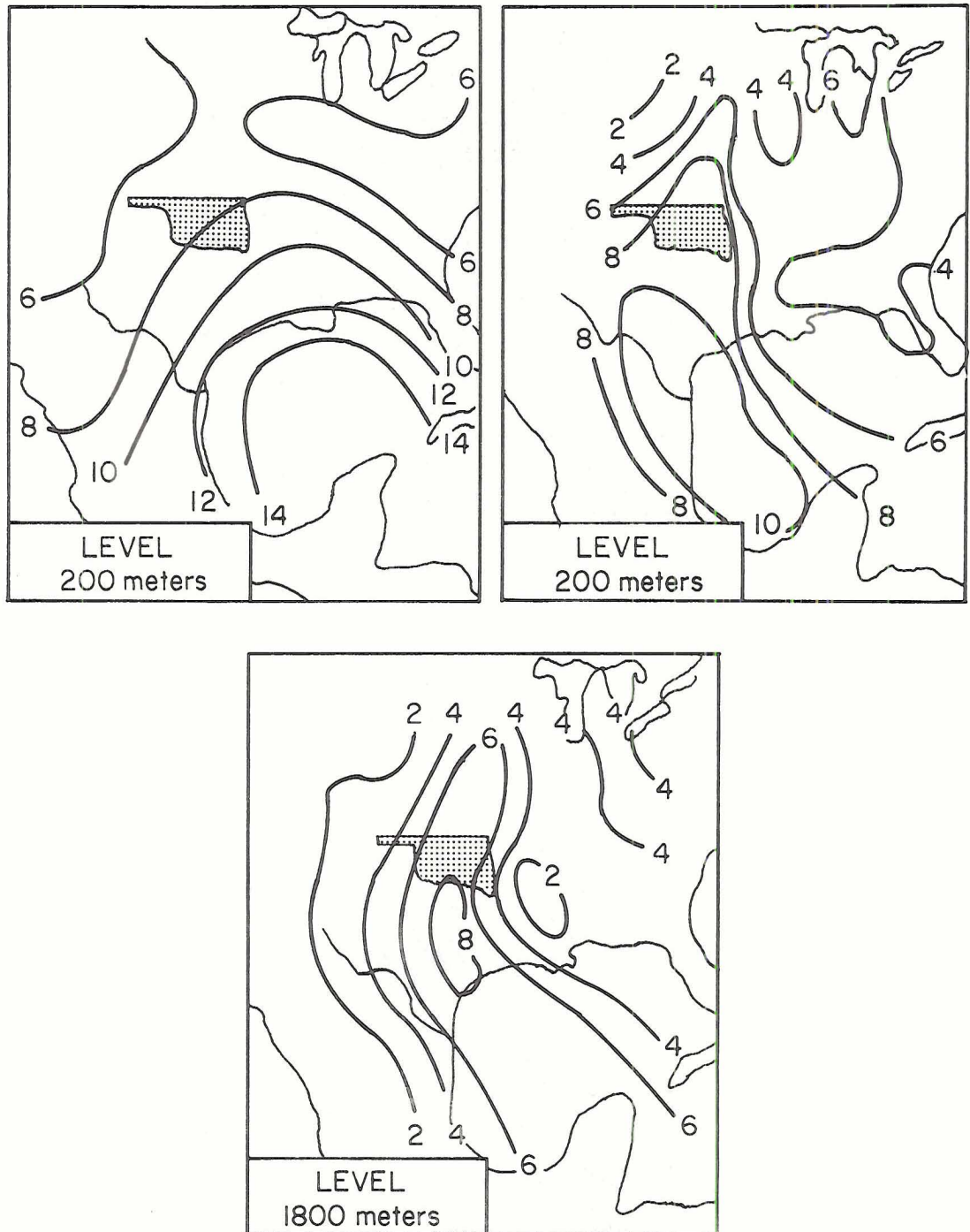
Fig. 6. Observed moisture (gm kg^{-1}) 0600 CST, 25 March 1967.
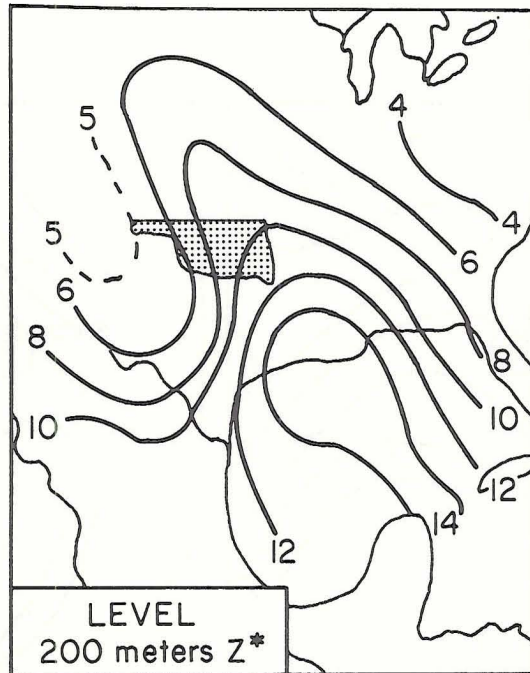
Fig. 7.   Forecasted moisture (gm kg^{-1})
1800 CST, 25 March 1967
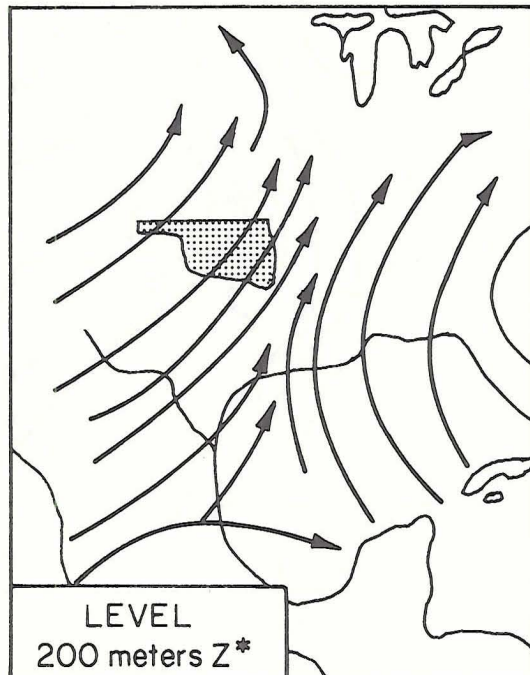
Fig. 8.   Forecasted streamline
1800 CST, 25 March 1967.
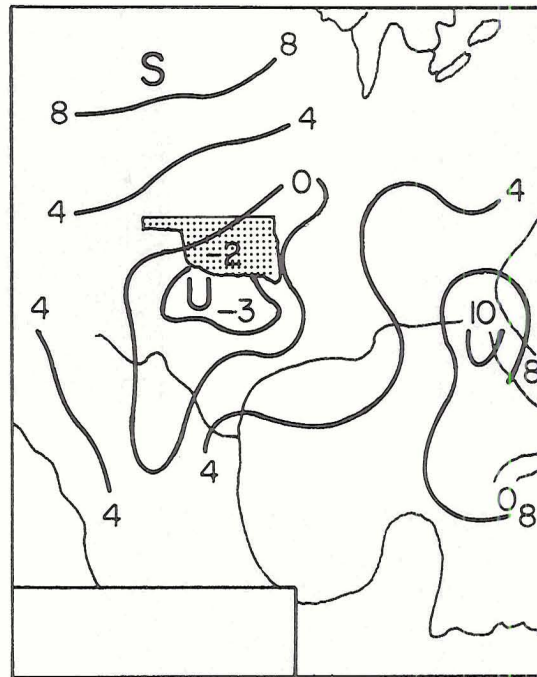
Fig. 9. Observed stability at
1800 CST, 25 March 1967
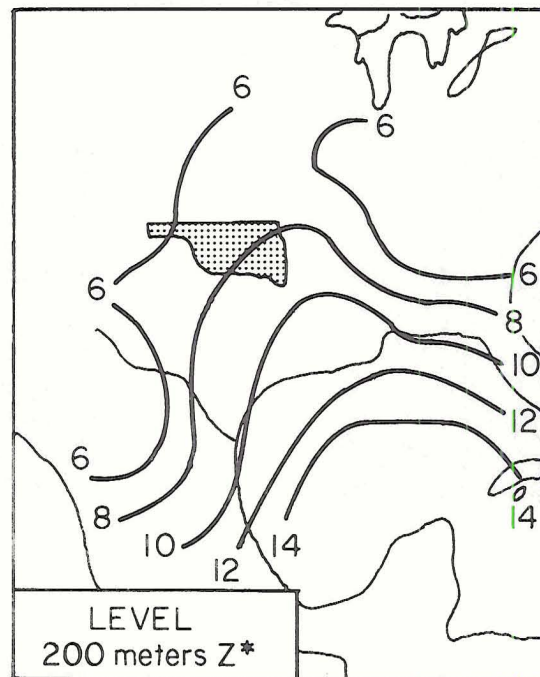
Fig. 10. Observed moisture (gm kg^{-1})
0600 CST, 25 March 1967
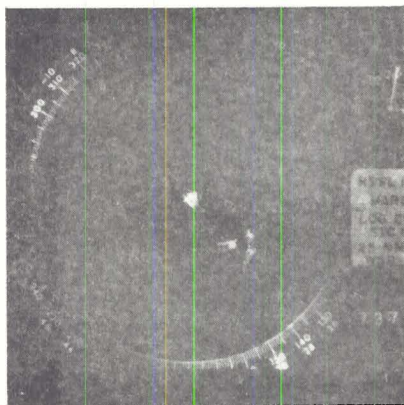
0600 CST

0900 CST
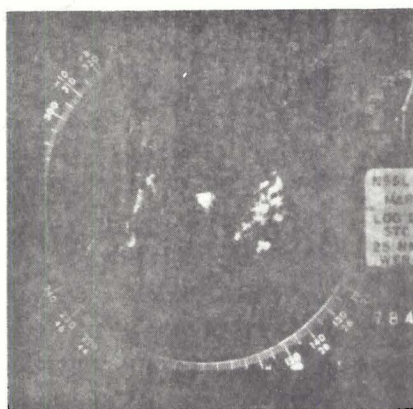
1200 CST
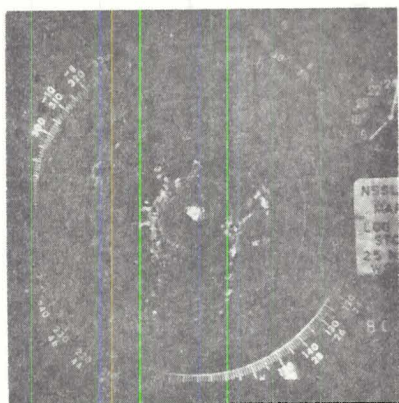
1500 CST
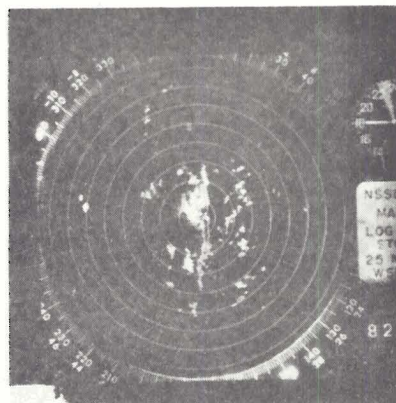
1800 CST

Fig. 11. Radar echo summary for 25 March 1967.
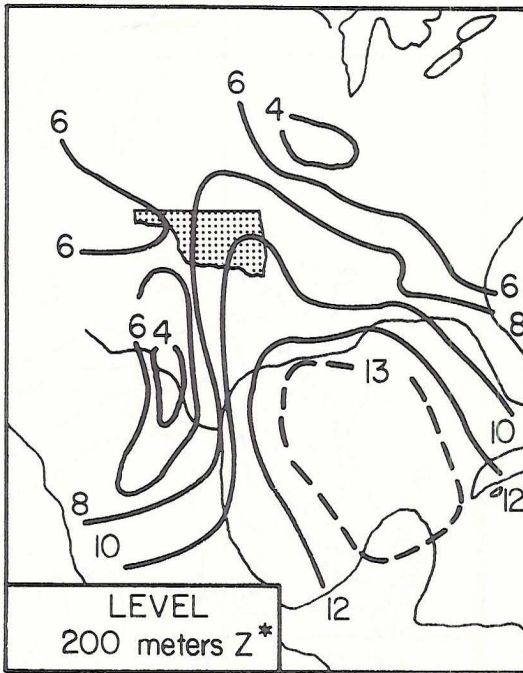
Fig. 12.   Observed moisture at
           1800 CST, 25 March 1967
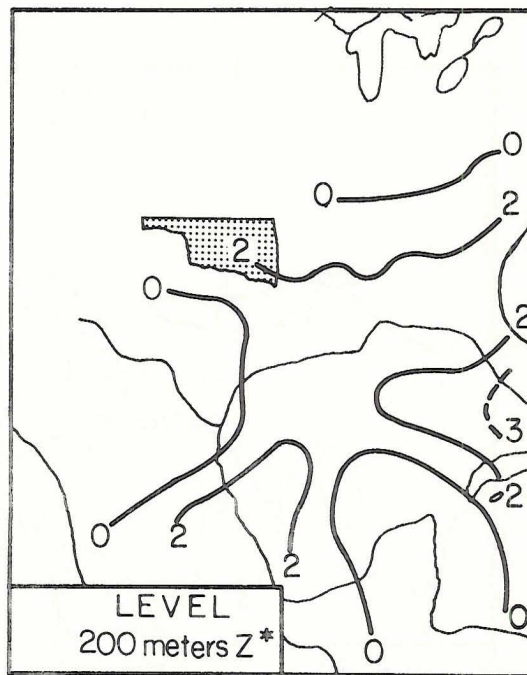
Fig. 13.   Verification of experiment
           1 on moisture, 1800 CST,
           25 March 1967.
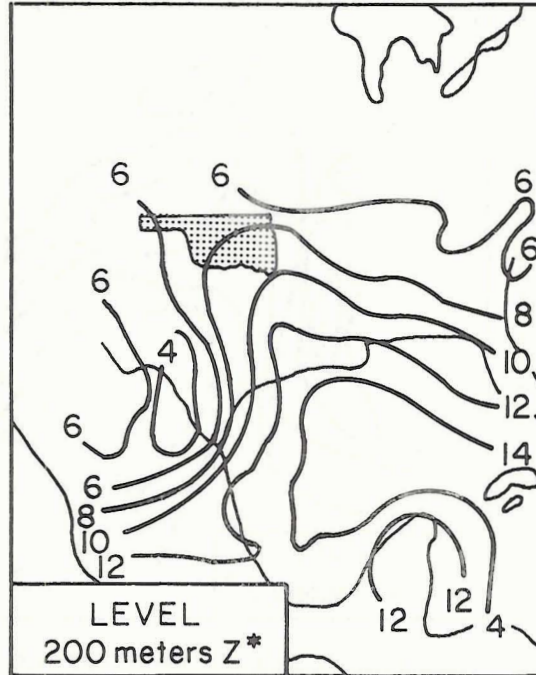
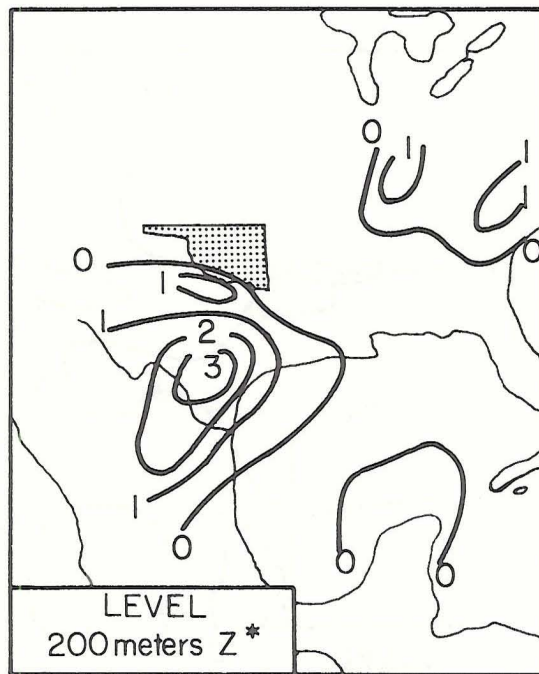Fig. 14. Forecasted moisture of
experiment 2, 1800 CST,
25 March 1967
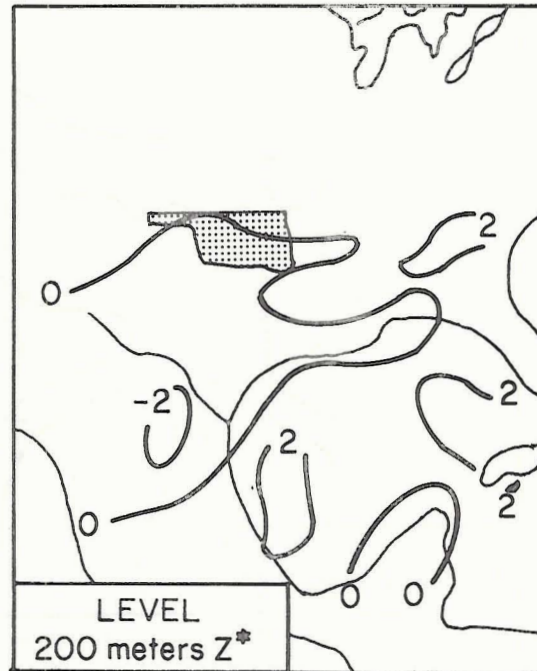
Fig. 15. Verification of experiment
2 on moisture, 1800 CST,
25 March 1967.

LEVEL
1000 meters Z*

1200 CST

LEVEL
1000 meters Z*
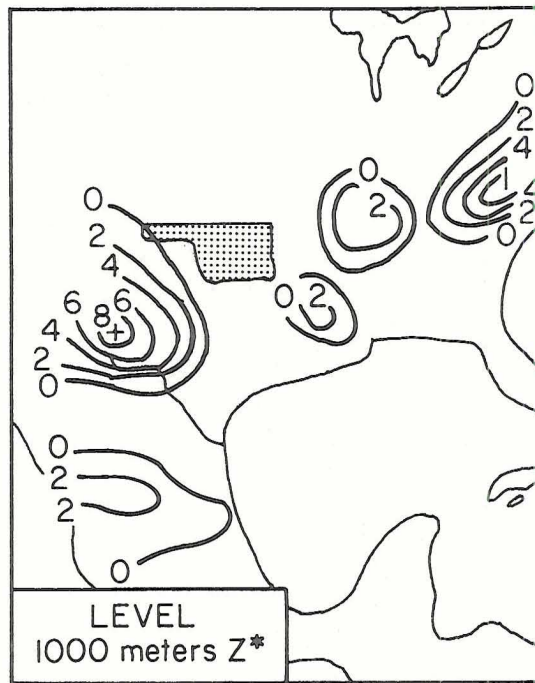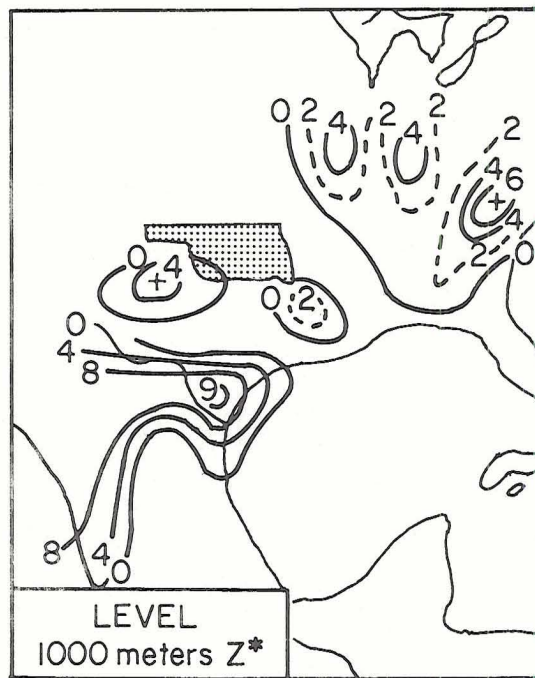
1800 CST, 25 March 1967

Fig. 16. Storm Index wq of experiment 2.
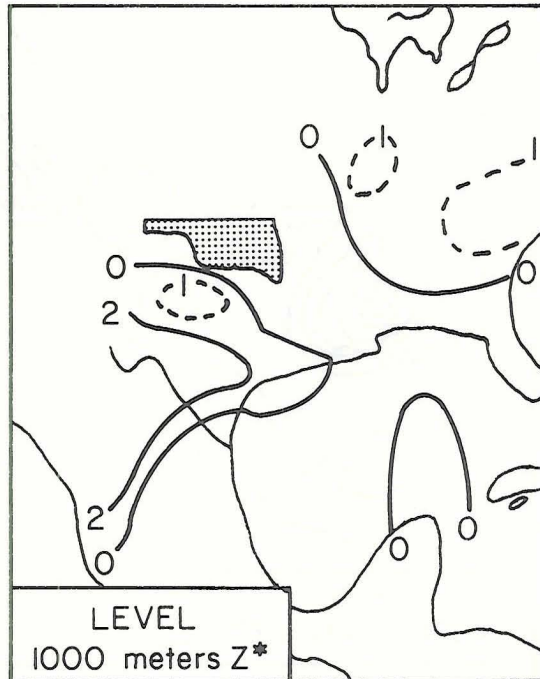
Fig. 17. Forecasted w (cm sec^{-1}) of experiment 2, 1800 CST, 25 March 1967
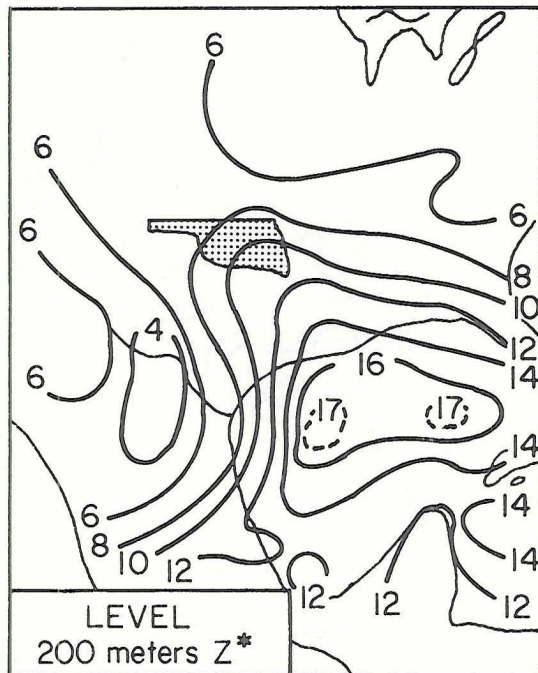
Fig. 18. Forecasted moisture of experiment 3, 1800 CST, 25 March 1967.
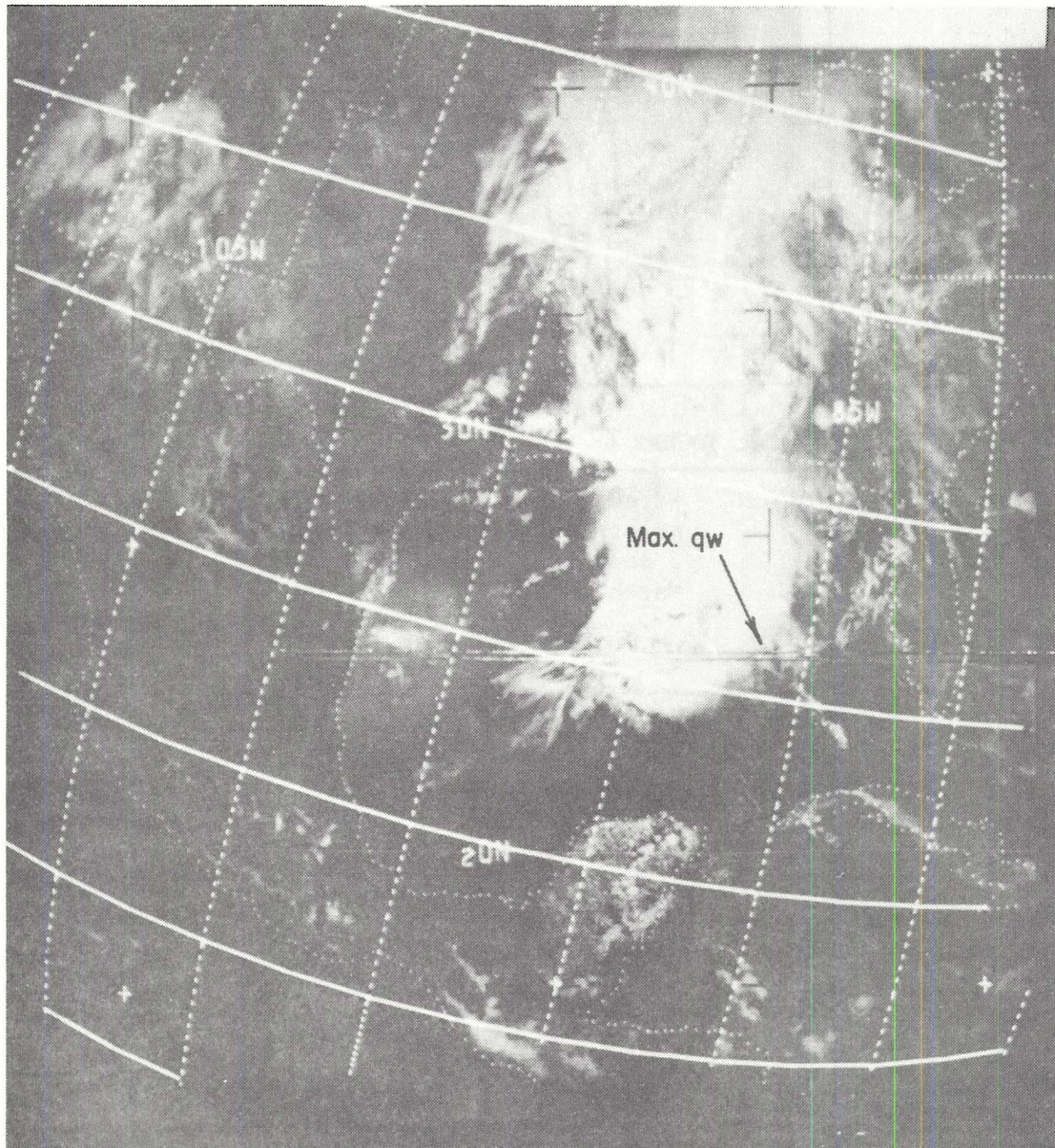
Fig. 19.   Satellite Photograph for 26 March 1967 at 1938GMT.
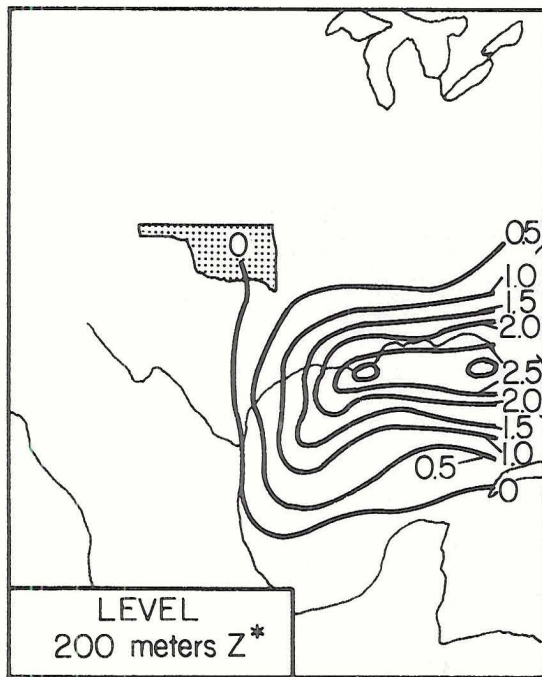
Fig. 20. Forecasted differences in
moisture between experiments
2 and 3, 1800 CST, 25
March 1967
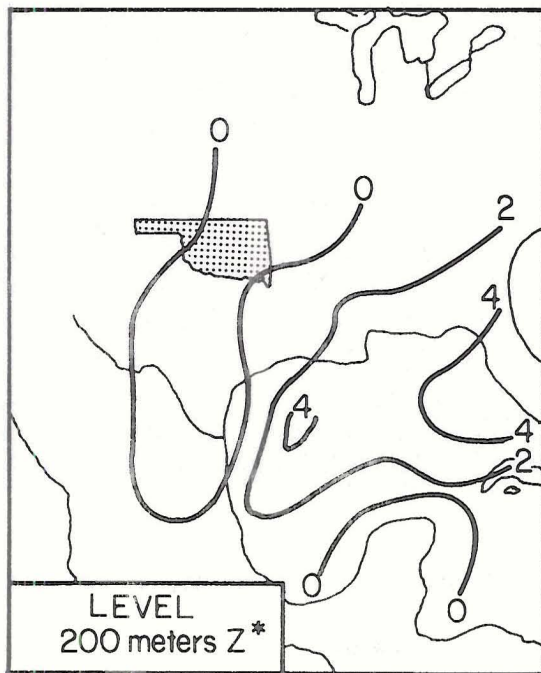
Fig. 21. Verification of experiment
3 on moisture, 1800 CST,
25 March 1967
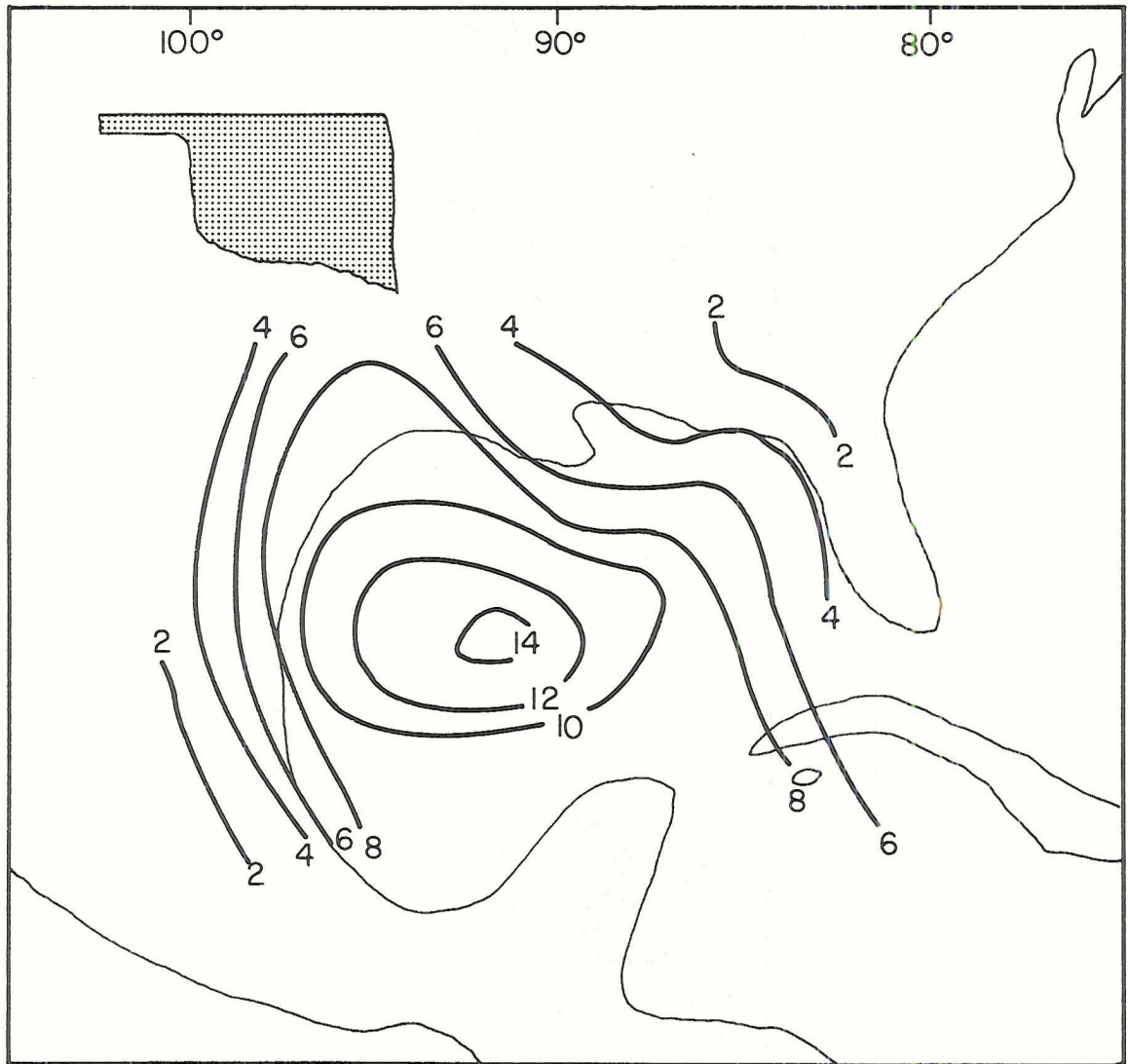
Fig. 22. Horizontal moisture transport qV_h (gm kg^{-1} cm sec^{-1} x 10^3)
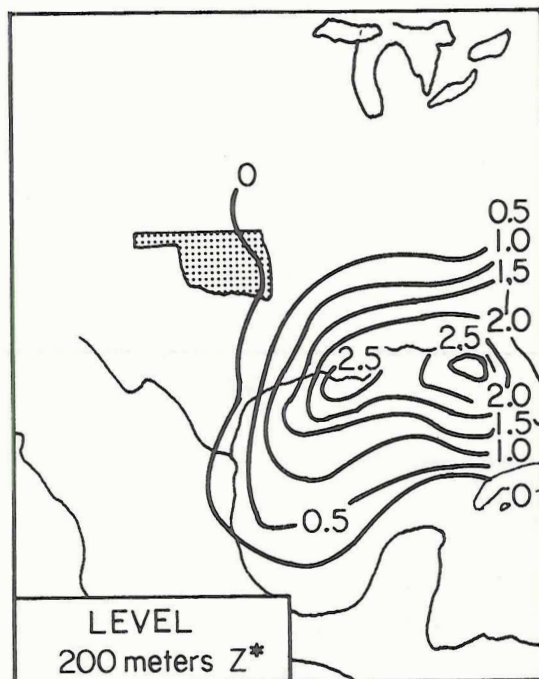
Fig. 23. Evaporation effects,
1800 CST, 25 March 1967,
without using topo-
graphical coordinate
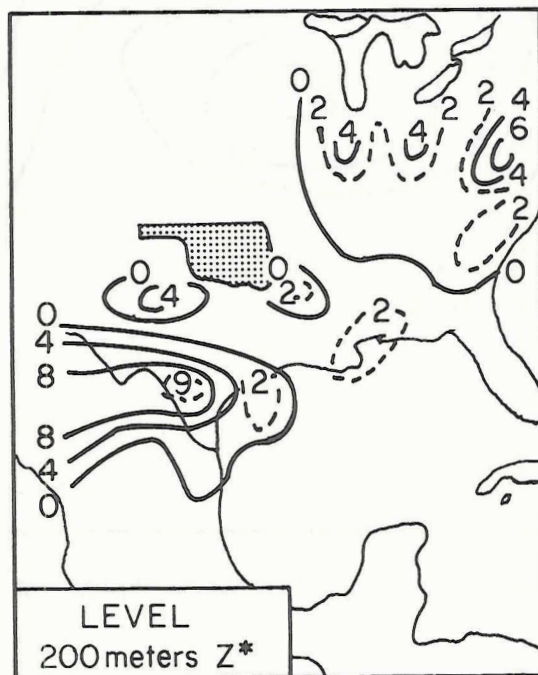
Fig. 24. Storm index wq of experiment
3, 1800 CST, 25 March 1967
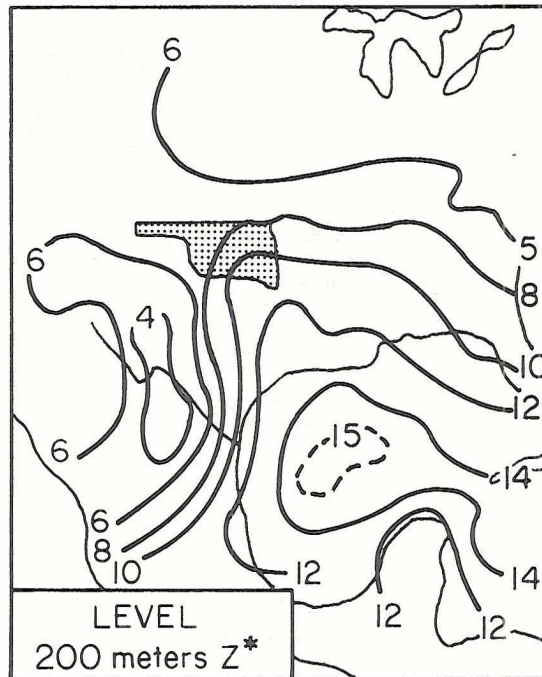
Fig. 25. Forecasted moisture of
experiment 4, 1800 CST,
25 March 1967
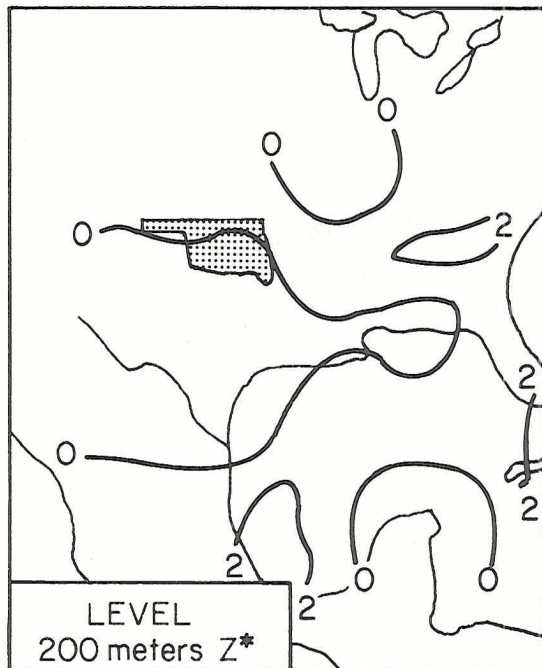
Fig. 26. Verification of experiment
4 on moisture, 1800 CST,
25 March 1967
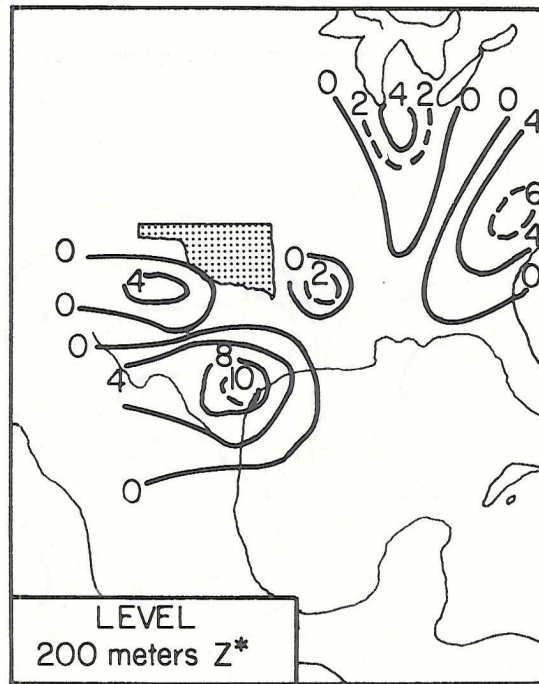
Fig. 27. Storm index wq of
experiment 4, 1800 CST,
25 March 1967

Fig. 28. Forecasted w (cm sec^{-1})
of experiment 4, 1800 CST,
25 March 1967
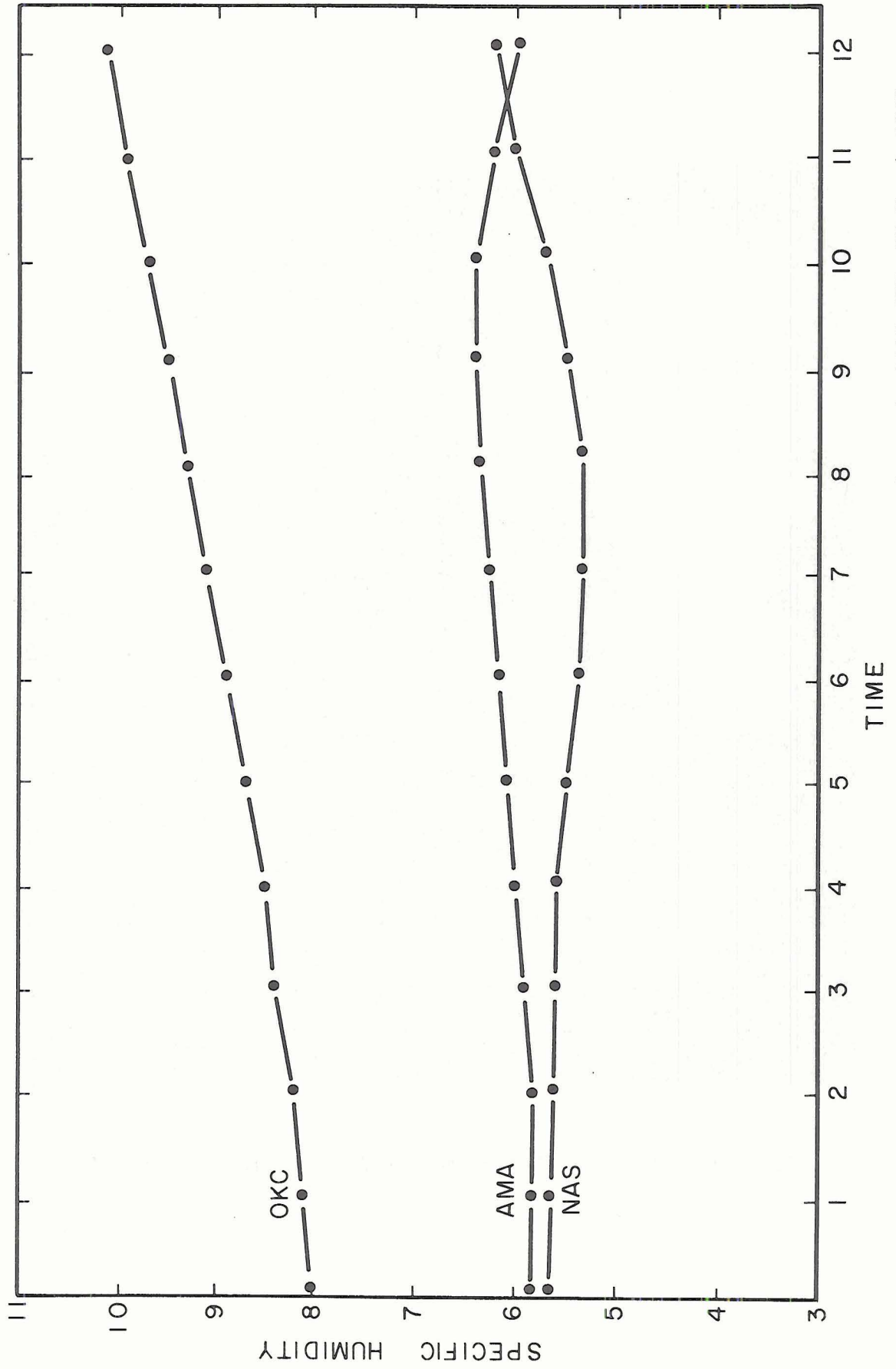
Fig. 29. Constant Tracking of Moisture of Experiment 4, 1800 CST, 25 March 1967
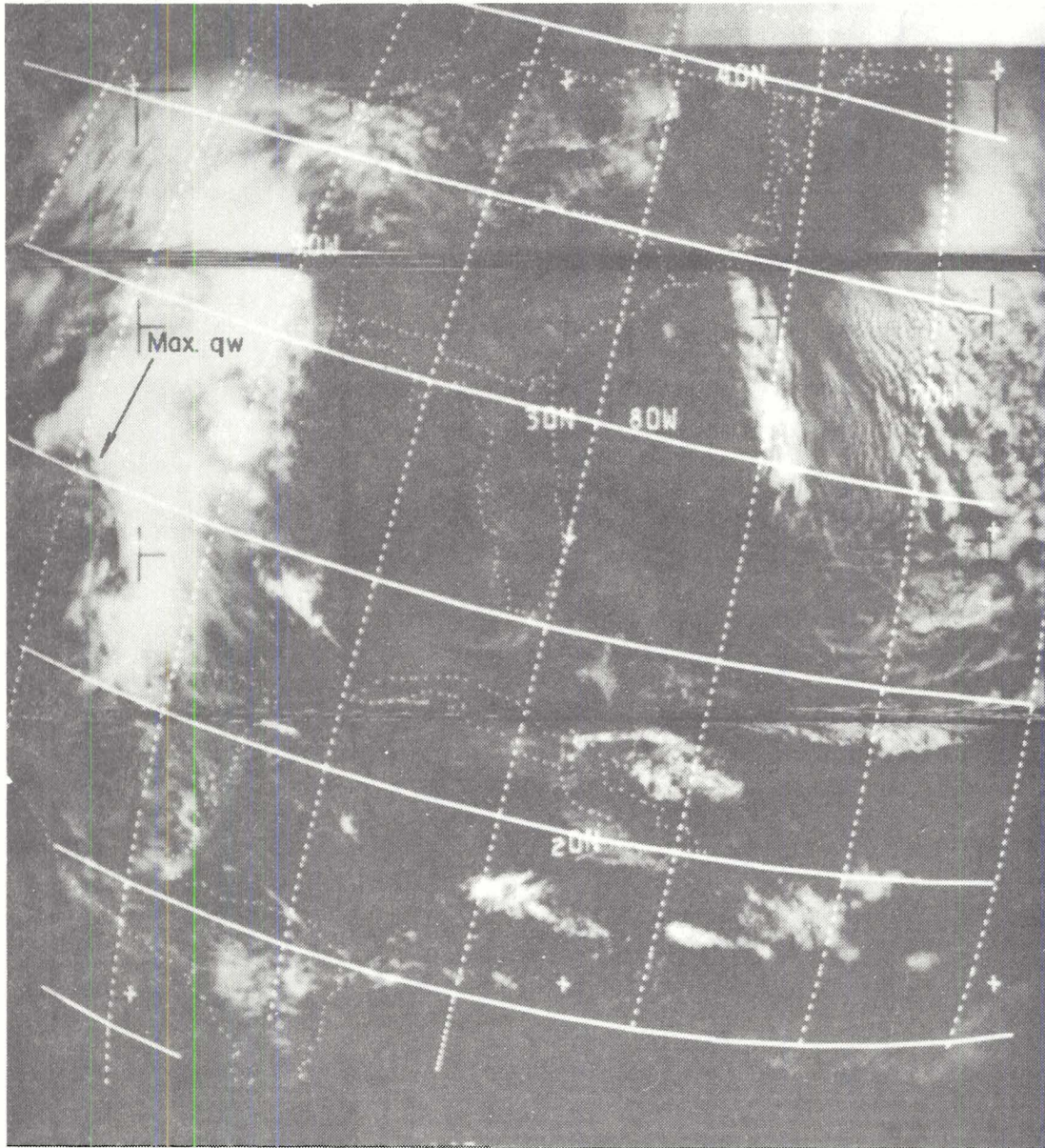
Fig. 30. Satellite Photograph for 25 March 1967 at 1847GMT.
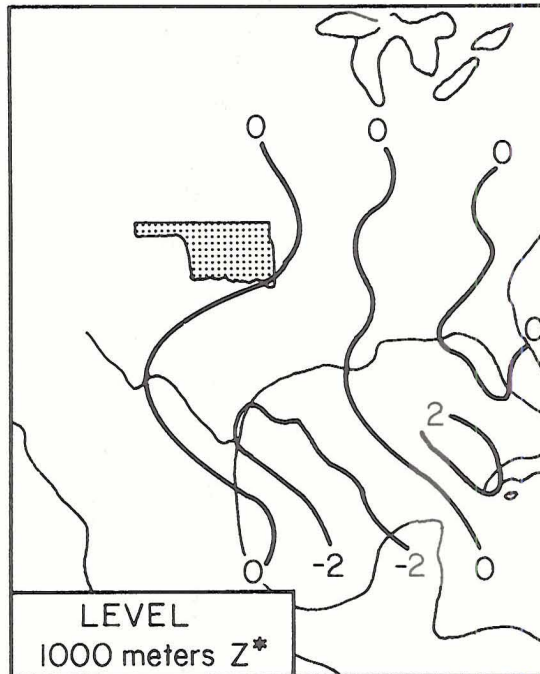
Fig. 31.   Verification of experiment
           4 on moisture at 1000
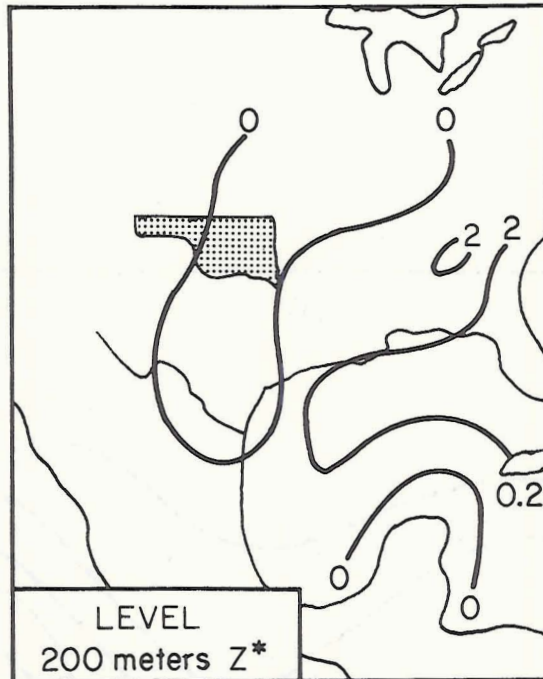   meters Z*, 1800 CST,
           25 March 1967
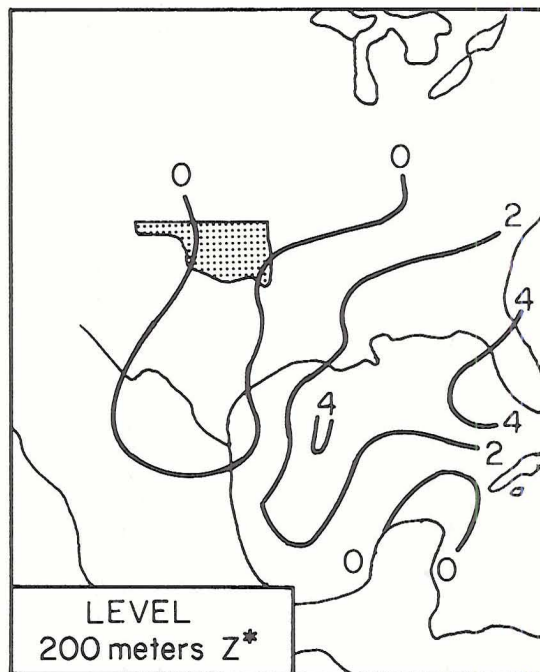
Fig. 32.   Verification of experiment
           4 on moisture accounting
           for evaporation, 1800 CST,
           25 March 1967
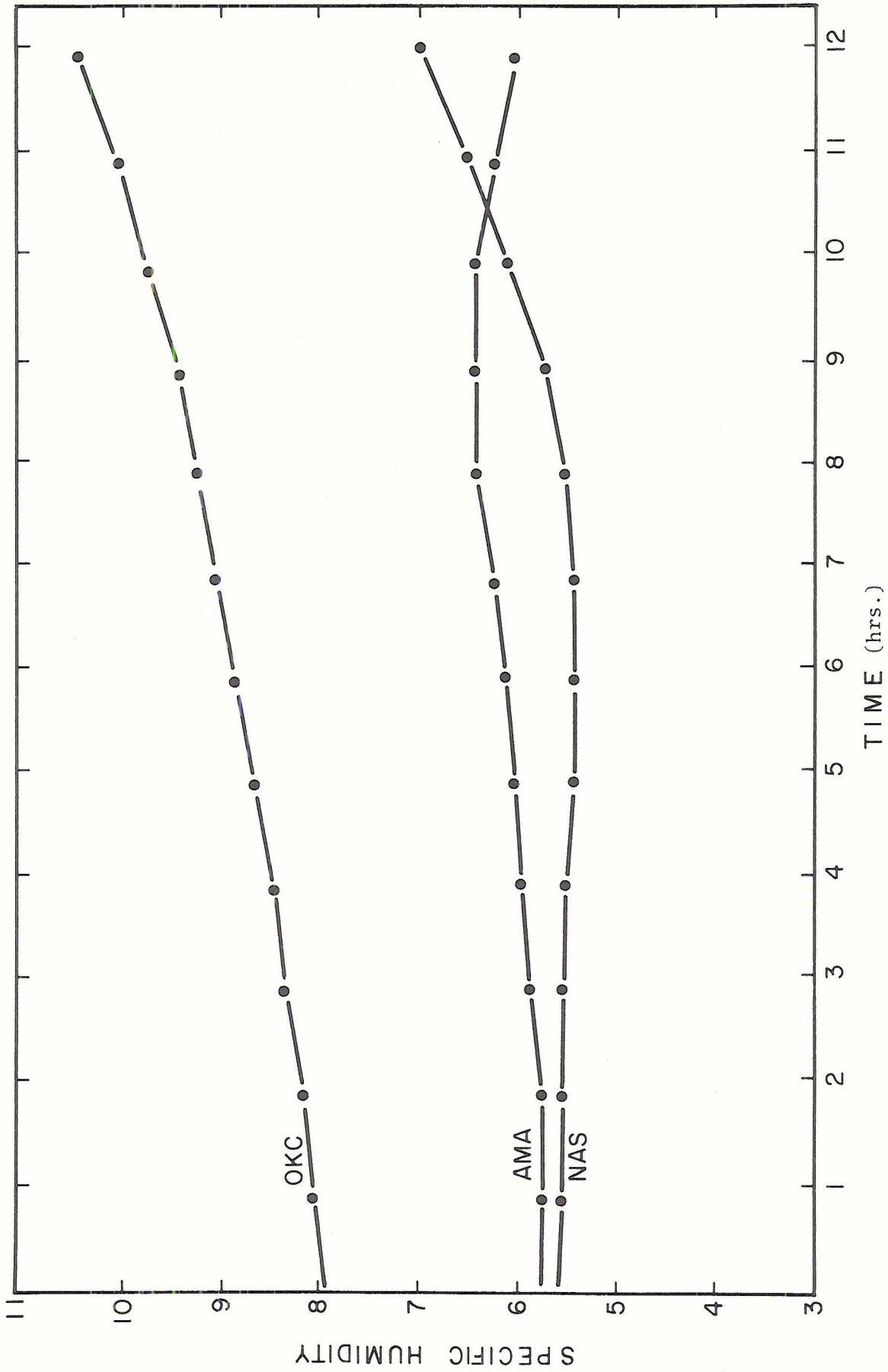
Fig. 33. Constant Tracking of Moisture of Experiment 4,
but accounting for Evaporation. 1800 CST,
25 March, 1967
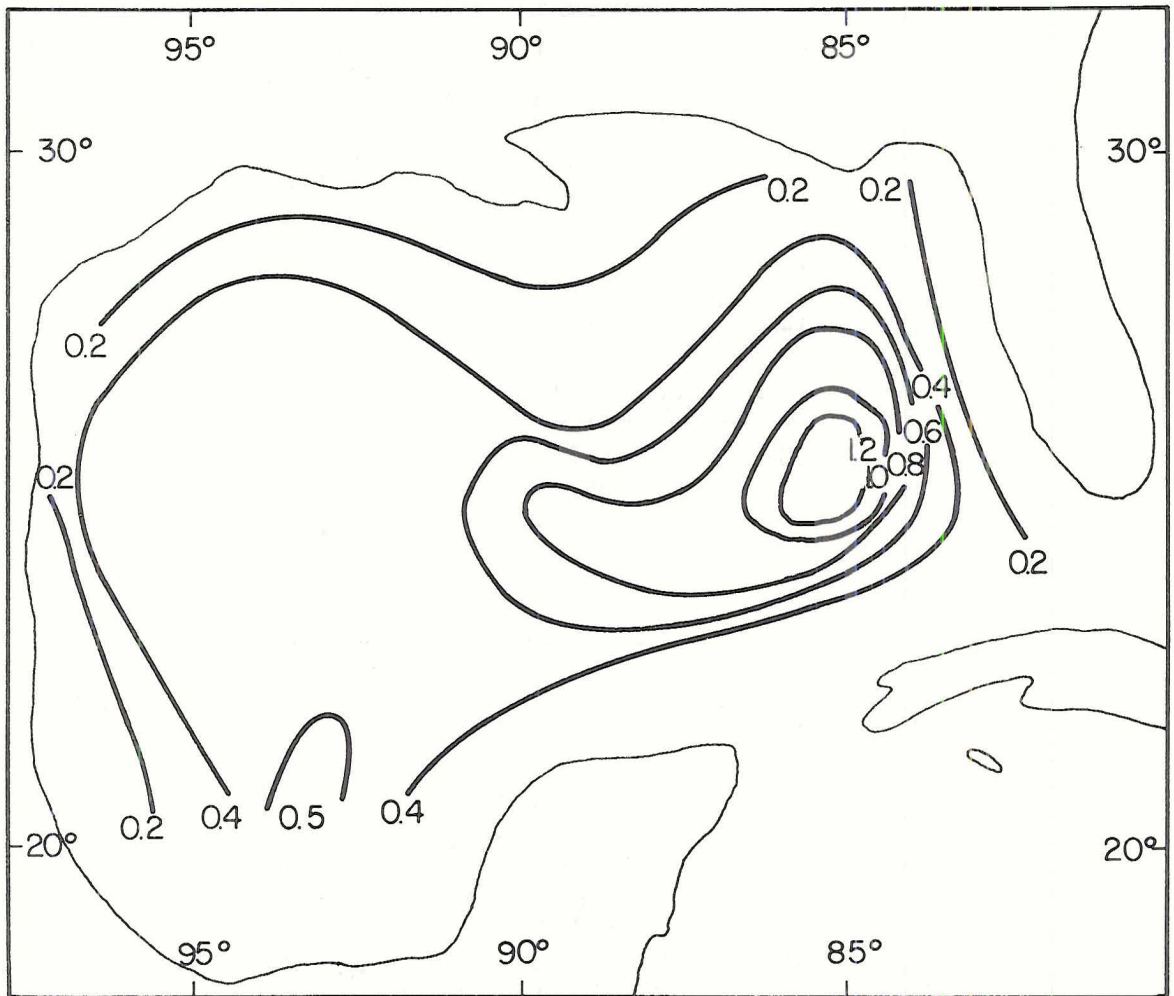
Fig. 34. Evaporation rate (gm cm^{-2} day^{-1})

Fig. 35. Verification of experiment
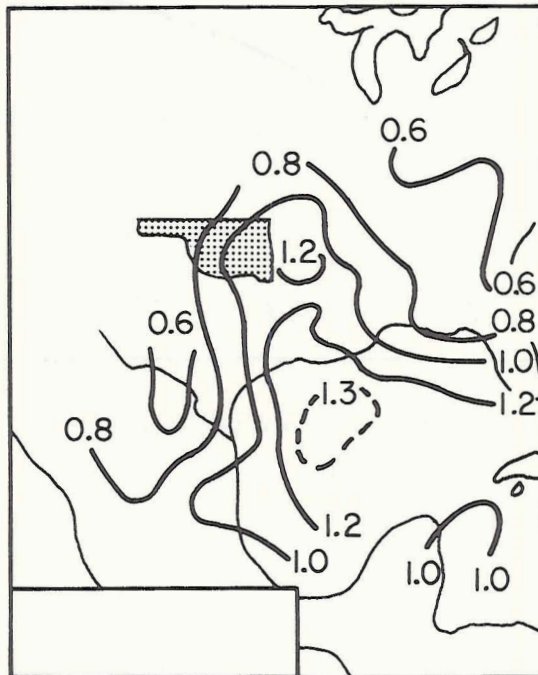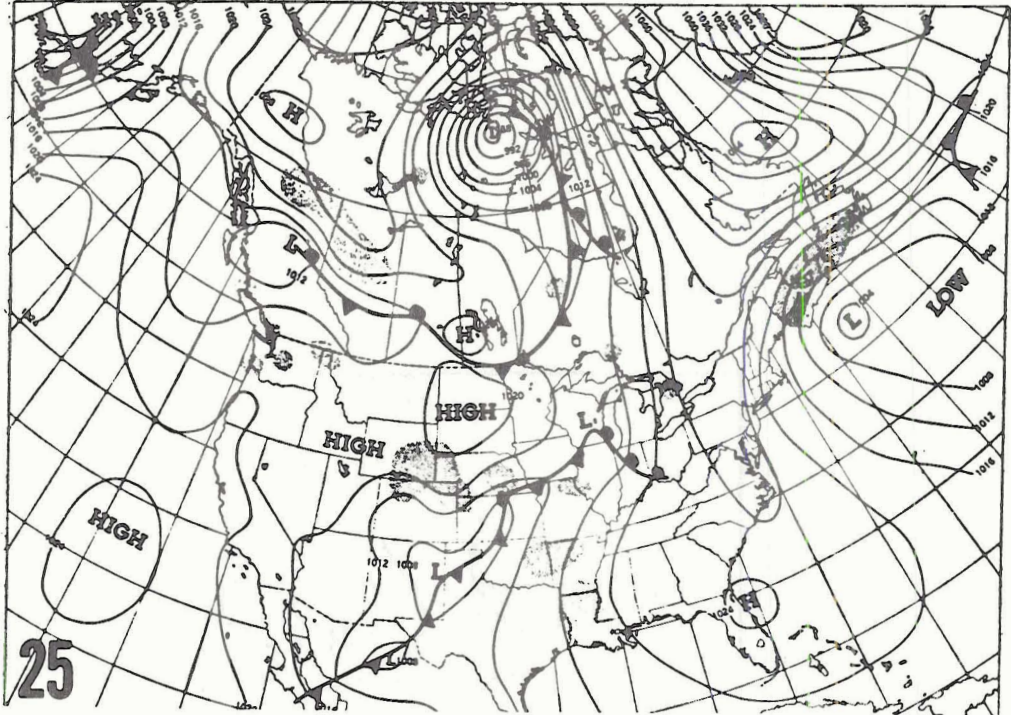4 on moisture accounting
for half of evaporation,
1800 CST, 25 March 1967

Fig. 36. Forecasted precipitable
water (gm cm^{-2}) of
experiment 4, 1800 CST,
25 March 1967

**Central Valley front produces R from Lakes to Gulf:
Kirksville, Mo. 1.09", Ft. Smith, Ark. .53", Waco .80"—
warmer Ohio Valley: 79°—coldest +8° in Pa., 89° Tex.**

Fig. 37.   Surface map at 1200 CST, 25 March, 1967.
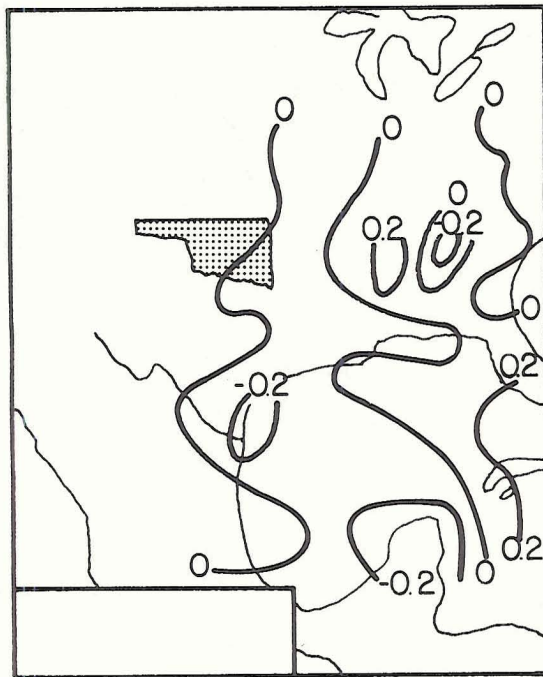Shaded areas indicate precipitation occurring
at map time.

Fig. 38.   Verification of
precipitable water.